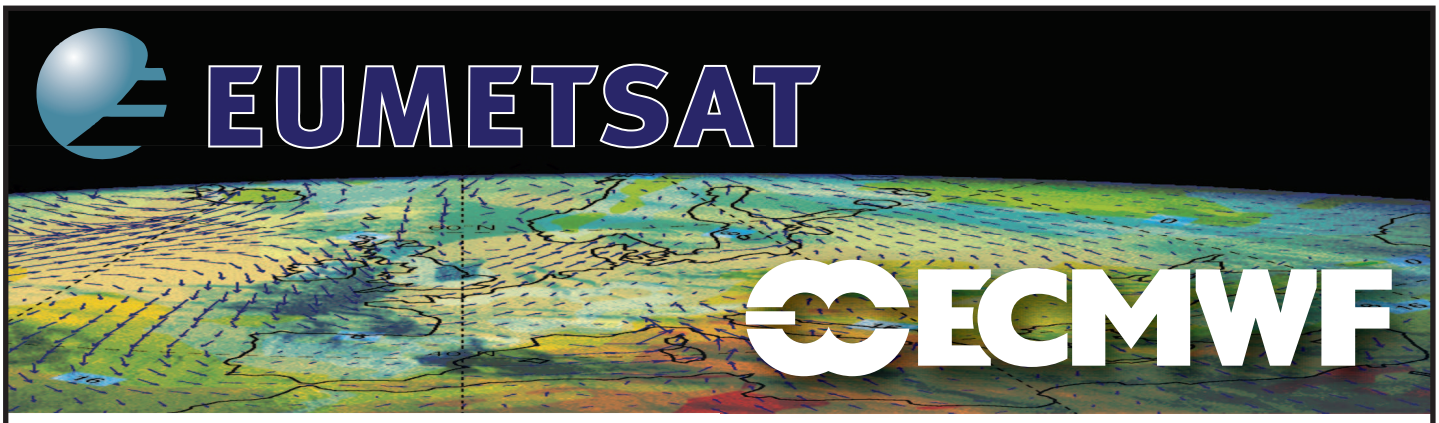

EUMETSAT/ECMWF Fellowship Programme
Research Report No. 30

All-sky assimilation of SSMI/S humidity sounding channels over land: second year report

F. Baordo A. J. Geer and S. English

September 2013

Series: EUMETSAT/ECMWF Fellowship Programme Research Reports

A full list of ECMWF Publications can be found on our web site under:
http://www.ecmwf.int/publications/

Contact: library@ecmwf.int

European Centre for Medium Range Weather Forecasts
Shinfield Park, Reading, RG2 9AX, England

Abstract

The all-sky assimilation of SSMI/S humidity sounding channels over ocean has been recently introduced within the ECMWF operational system, benefiting winds and humidity analysis and forecasts. The upgrade over ocean was based on better scattering radiative transfer calculations which, using discrete dipole simulations to represent optical properties of snow hydrometeors, improve the simulated microwave radiances. Taking advantage of such improvements, the all-sky package over ocean has been extended in order to have an equivalent framework to also assimilate SSMI/S humidity sounding channels over land. This paper not only describes the necessary technical changes to develop the over land framework, but also scientifically evaluates, through different assimilation experiments, the impact on analysis and forecast. The findings of this investigation show that the all-sky assimilation over land is reliable and it brings positive improvements into the system which can be seen in term of both forecast scores and fits to conventional and other satellite observations. These results encourage additional investigations to widen the application of the all-sky approach over land to other microwave humidity sounding sensors such as MHS.

1 Introduction

The possibility of extending the well establish all-sky framework over ocean (Geer and Bauer, 2010, 2011, Bauer et al., 2010) to land surfaces was initially investigated during the first year of the fellowship and it was documented by Baordo et al.(2012). The results of that investigation were mainly two: a) it is feasible to consider a land surface emissivity retrieval from satellite observations in all-sky conditions; b) deficiencies in radiative transfer calculations, mainly due to the use of Mie sphere to represent frozen hydrometeors, generally restrict developments of assimilating higher microwave frequencies such as SSMI/S humidity sounding channels.

Recently, in order to obtain more realistic simulated brightness temperature, Geer and Baordo (2013) investigated the choice of modelling scattering radiative transfer using discrete dipole approximation (DDA) to represent optical properties of snow hydrometeors. This study found that the use of DDA sector snowflakes (Liu, 2008) to represent the optical properties of snow hydrometeors, improves the global simulation of microwave radiances compare to the inappropriate assumption of Mie spheres. The modified all-sky package over ocean will be introduced in the IFS cycle 40r1 and the benefits obtained are documented by Geer (2013). In the same way, the advantages of better radiative transfer calculations have been additionally exploited in order to build an equivalent framework to also assimilate SSMI/S humidity sounding channels over land in all-sky conditions. Hence, the second year of the fellowship has aimed at achieving this goal.

The report is organised in two parts: the first part describes the necessary technical and scientific changes in order to develop the all-sky package over land; the second part analyses the scientific impact of assimilating SSMI/S humidity sounding channels by means of experimentation within the ECMWF system.

Developments of the all-sky package over land are summarised in the following paragraphs as listed below:

- section 2: a general overview of the all-sky assimilation is given.
- section 3: improvements of radiative transfer calculations for SSMI/S humidity sounding channels over land are described.
- section 4: details on the observation error modelling are provided.

- section 5: surface emissivity estimates used in the all-sky framework over land are analysed.

In section 6, scientific impact of the all-sky assimilation over land has been explored. The evaluation is carried out by using a control experiment that contains the changes of the all-sky over ocean package Geer (2013). Firstly, the impact of the all-sky assimilation is evaluated against an equivalent experiment that uses cloud screening. Secondly, the reliability of the all-sky framework over land is investigated by means of other experiments having slightly different configurations. Finally, surface screening impact is also evaluated. General conclusions are discussed at the end of the report.

2 All-sky assimilation general overview

The observation operator designed for assimilating microwave radiances in all-sky conditions is RTTOV-SCATT (Bauer et al., 2006). This uses the delta-Eddington approximation (Joseph et al., 1976) to solve the radiative transfer equation including scattering. Two liquid and two frozen hydrometeors types are provided by IFS to RTTOV-SCATT: cloud water, rain, cloud ice and snow. The optical properties of each particle are taken from look-up tables: cloud water, rain and cloud ice are considered as a sphere and modelled using Mie theory, while snow hydrometeors, as described in section 3, are represented by DDA sector snowflakes (Liu 2008). Land surface emissivity is retrieved from satellite observations (Baordo et al., 2012) and assessed by emissivity estimates from TELSEM (Tool to Estimate Land Surface Emissivities at Microwave frequencies, Aires et al., 2010), a package available within RTTOV, containing pre-calculated monthly mean emissivity climatology derived from ten-year SSM/I observations. Ocean surface emissivity is computed using version 5 of FASTEM (Liu et al., 2011). The simulated brightness temperature is computed considering the contribution from two independent sub-columns: a clear column, taking into account only gaseous absorption, and a cloudy column additionally taking into account cloud, precipitation and scattering. The two sub-columns are weighted according to the effective cloud fraction (Geer et al., 2009), depending not only on the hydrometeor amount (cloud liquid, cloud ice, rain and snow) but also on the convective and large-scale precipitation fractions at each layer of the atmosphere. All-sky assimilation is operationally implemented over ocean for SSMI/S observations (Kunkee et al., 2008) on DMSP satellite F17 and TMI (Kummerow et al., 1998) on TRMM. SSMI/S observations are pre-processed to eliminate calibration anomalies according to Bell et al. (2008). Observations are also averaged in boxes of approximately 80 km by 80 km in order to make the horizontal scales of observed cloud and precipitation more similar to their effective resolution in the model. Complete details of the all-sky assimilation are given by Geer and Bauer (2010, 2011) and Bauer et al. (2010).

3 Improvement of radiative transfer calculations

Deficiencies in radiative transfer calculations, mainly due to the use of Mie sphere to represent frozen hydrometeors, have restricted developments of all-sky assimilation wherever scattering effects are dominant (for instance over land surfaces or in temperature and humidity sounding channels). Recently, in order to obtain more realistic simulated brightness temperatures, Geer and Baordo (2013) investigated the choice of which DDA particle shape is optimal to represent the optical properties of snow hydrometeors in the all-sky radiative transfer calculations. To objectively guide this choice, the authors used observation minus forecast statistics from the ECMWF system. In order to reduce complexity, the particle size distribution stayed fixed (the tropical version of the Field et al. 2007 was used), while the shape was varied. The main goal of the study was concentrated on finding one globally-applicable DDA

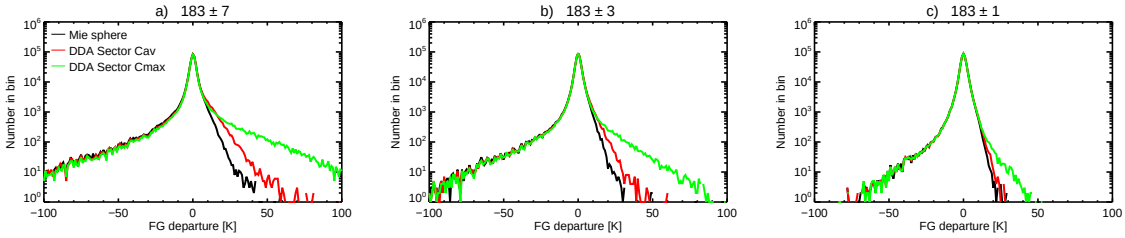

Figure 1: Histograms of FG departure [K] for the month of June 2012 using Mie sphere snow and DDA sector snow with 'Cav' or 'Cmax' approach, for the SSMI/S channels at 183±7 GHz, 183±3 GHz and 183±1 GHz. Bin size is 2.0 K; y axis is logarithmic. Sample of observations is over land between 60°S and 60°N.

shape to represent snow hydrometeors in order to improve radiative transfer calculations. The study also looked for a DDA shape to represent cloud ice and investigated the use of different shapes for convective and large-scale snow. However, snow hydrometeors are more important for two reasons: a) snow particles are generally larger than ice particles and hence more effective at scattering; b) the ECMWF model produces much less cloud ice than snow. The findings of the study show that modelling snow hydrometeors with Liu sector snowflakes (hereafter mentioned as DDA sector or sector only) provides the best fit between the ECMWF model and observations, considering all SSMI/S channels between 10 GHz and 183 GHz. The results also show that benefits of using more complex DDA configurations are minimal compared to the simpler sector configuration. Considering the aim of this report, we only summarise the DDA radiative transfer impact on SSMI/S humidity sounding channels over land, but for more details the reader might refer to Geer and Baordo (2013).

The impact of DDA shapes on simulated brightness temperatures has been evaluated within the ECMWF system by means of assimilation experiments which have the same configuration except the use of different look-up tables for optical properties of snow hydrometeors (i.e. Mie sphere or a particular DDA shape). In all the experiments observations over land are passive. To isolate the impact of land surface emissivity on the resultant simulated radiances, radiative transfer calculations have been carried out using emissivity estimates from TELSEM. In this way computations are not affected by emissivity biases and the outcomes can be equally compared. As mentioned in section 2, simulated all-sky brightness temperatures over ocean are computed and weighted according to the effective cloud fraction (hereafter mentioned as 'Cav'). However, this approach has not previously been tested over land surfaces. For this reason, beside the use of 'Cav', DDA sectors have been also tested with the old 'Cmax' approach, which takes the largest cloud fraction in the model profile to represent the effective cloud fraction.

Figure 1 shows histograms of FG departure for the month of June 2012 using Mie sphere snow and DDA sector snow with 'Cav' or 'Cmax' approach for the SSMI/S humidity sounding channels. The sample of observations is composed of SSMI/S data over land between 60°S and 60°N. Using the Mie sphere to represent snow hydrometeors produces insufficient scattering leading mainly to negative departures (tail of negative departure well defined) and very few positive departures (tail of positive departure completely missing). Using DDA sector for snow produces more scattering, hence simulated brightness temperatures are colder and as a result there is a much more symmetrical distribution of FG departures. The use of 'Cmax' rather than 'Cav' might be scientifically questionable (this is discussed at the end of this section), but it is practically helpful. 'Cmax' produces always higher effective cloud fractions than the 'Cav' approach and, as a consequence, the weight given to the cloudy column in RTTOV-SCATT increases, thus increasing the amount of scattering affecting the simulated brightness temperatures. Difference between the use of Mie sphere and sector for snow is also channel dependent being more obvious at

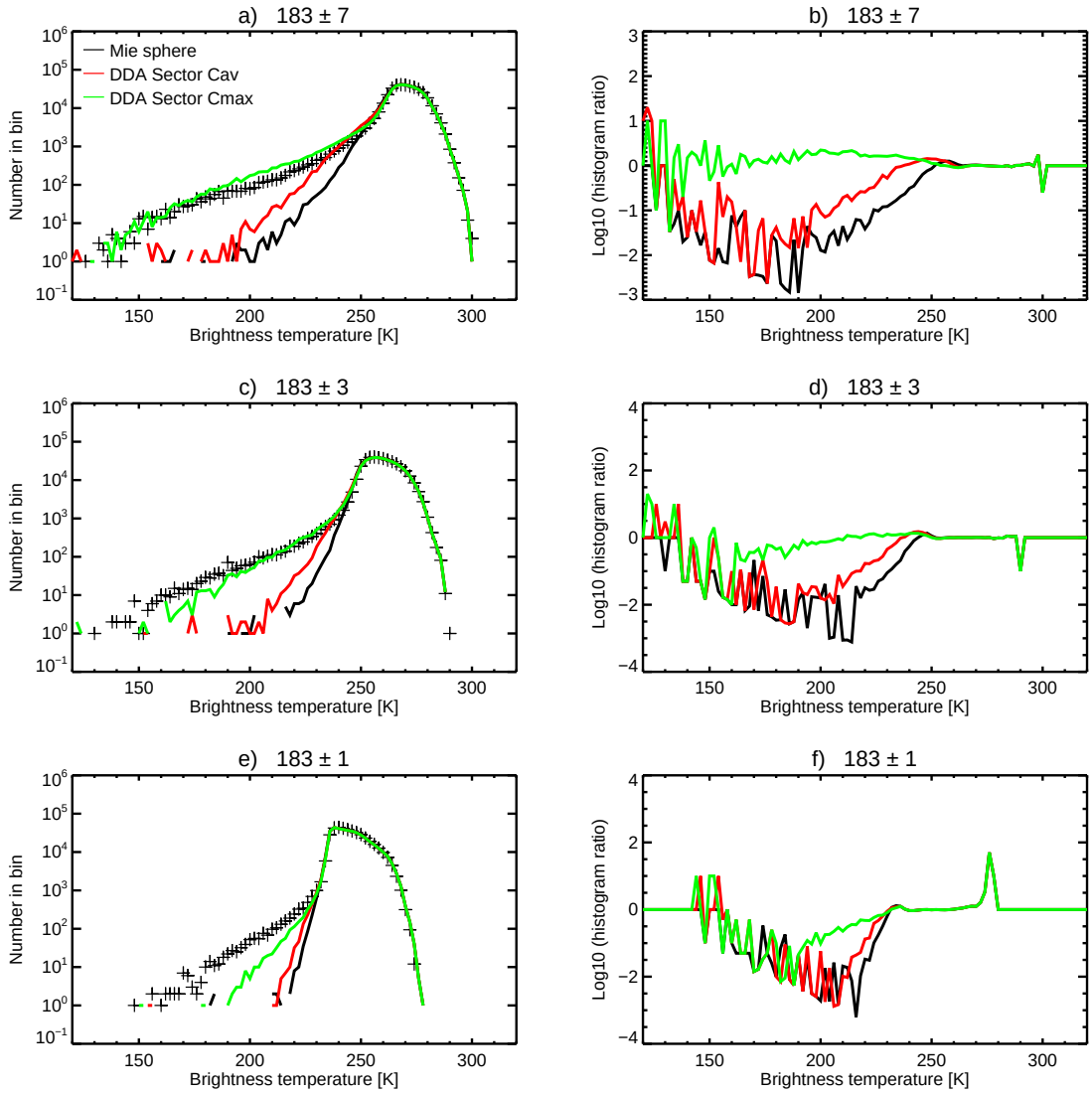

Figure 2: Measure of histogram fits for the month of June 2012 for SSMI/S channels at 183±7 GHz, 183±3 GHz and 183±1 GHz. (a, c, e) Histogram of observed (black cross) and simulated (colour line) brightness temperatures [K] using Mie sphere snow and DDA sector snow with 'Cav' or 'Cmax' approach. Sample of observations is over land between 60°S and 60°N. Bin size is 2.0 K. (b, d, f) Log of the ratio of histograms (simulation divided by observation). Empty bins have been filled with the 0.1 value to prevent infinite value.

	Mie sphere	DDA sector 'Cav'	DDA sector 'Cmax'
Freq (GHz)	**Skewness of FG departures**		
183±7	-6.18	-3.41	1.01
183±3	-6.68	-5.32	-1.22
183±1	-4.11	-3.67	-2.77
	RMS of FG departures [K]		
183±7	6.98	7.31	9.68
183±3	4.99	5.15	5.97
183±1	3.33	3.37	3.47
	Brightness temperature histogram fit (h)		
183±7	1.06	0.76	0.22
183±3	1.17	0.89	0.33
183±1	1.09	1.01	0.69

Table 1: Summary of the statistics used to optimise the choice between DDA sector 'Cav' or 'Cmax'. Statistic are based on SSMI/S observations over land between 60°S and 60°N for the month of June 2012.

183±7 and 183±3 than 183±1. This is reasonable considering that 183±1 is more sensitive to upper tropospheric layers and, as a consequence, cloud and precipitation is observed less frequently than in channels that sound deeper.

A second way to evaluate the impact of using DDA sector is given in Figure 2a, 2c and 2e, where histograms of observed and simulated brightness temperature are compared. It is again obvious that the Mie sphere simulations are inappropriate, because they are not able to produce brightness temperatures lower than 200 K, while some observations can be even lower than 150 K. The use of DDA sector and 'Cav' approach generates colder simulated radiances (some occurrences lower than 200 K), but the best fit to the observation distribution below 230 K is provided by the 'Cmax' approach. Again improvements at 183±1 are not as good as the other two channels. To better identify differences between the approaches, Figure 2b, 2d and 2f show the log ratio corresponding respectively to the histograms of Figure 2a, 2c and 2e (the ratio of population in each bin given by the number of simulated divided by the number of observed. Empty bins are assigned a population of 0.1 to prevent infinite ratios). The nonphysically warm radiances produced by Mie simulations are penalised by log ratio values between -1 and -3 in bins below 230 K. In general, the smaller the penalty in the bins the better is the agreement between observations and simulations: the smallest values are clearly observed when DDA sector and 'Cmax' approach is used.

To additionally compare the three approaches in a statistical sense, Table 1 summaries the statistics used to quantify changes in the resultant simulated radiances:

1. skewness of FG departures;
2. RMS (Root Mean Square) of FG departures;
3. brightness temperature histogram fit (h): the absolute value of the log ratio given by the sum across all bins and divided by the number of bins in which observations occur.

The skewness of FG departures indicates which approach brings a more symmetric distribution (skewness close to zero), while brightness temperature histogram fit can help to indicate wherever changes in

RMS of FG departures have occurred for good or bad reasons. The use of 'Cmax' produces the smallest values of h which indicates less discrepancies between simulated and observed radiances. Hence, the larger RMS of FG departures can be justified (summary in Table 1). The overall result suggests that DDA sector and 'Cmax' seems to be the best configuration to improve radiative transfer calculations over land, not only for humidity sounding frequencies, but in all channels between 10 GHz and 183 GHz (results not shown here). The use of 'Cmax', as mentioned before, might be questionable considering the more physical realism of the 'Cav' approximation. Firstly, 'Cav' works very well over ocean surfaces, and, secondly, the results over land from 'Cav' were much better in agreement with the more accurate radiative transfer calculations using the multiple independent column approach (ICA). Within the ICA, the grid box is divided into multiple-sub-columns (twenty sub-columns, in the test done) and the cloud and precipitation is distributed among those sub-columns according to cloud overlap rules (O'Dell et al., 2007). As pointed out in Geer and Baordo (2013), the discrepancy between land and ocean surfaces in terms of simulated radiances might be a model bias. For instance, occurrences of observed brightness temperatures (TB) at channel 183 ± 1, with TB less than 230 K, show that low radiances over land are more common than over ocean (i.e 0.94 % and 0.47 % at all observations over land and ocean, respectively). Within these occurrences, the percentage of model first guess snow water path (SWP) greater than 2 kg/m^2 over land is always about three times smaller than over ocean (i.e 9.90 % and 25.92 % over land and ocean, respectively). Looking at all simulations, the overall percentage of SWP greater than 2 kg/m^2 is 1.20 over land and 1.54 over ocean. These statistics suggest that the forecast produces less deep convection over land than over ocean in contrast to observations which indicate more convective areas over land. This might explain the beneficial impact of the 'Cmax' approach over land which helps to increase the amount of scattering producing colder simulated brightness temperatures.

Physical differences or discrepancies in forecast model bias between ocean and land should be investigated in more detail as well as other possible errors in the radiative transfer model that might only affect land surfaces. However, DDA sector and 'Cmax' give the best fit to observations and the technical implementation within IFS is also straightforward as long as the cloud overlap is varied from 'Cav' to 'Cmax' according to whether the surface is ocean or land. The all-sky assimilation of SSMI/S humidity sounding channels over land has been developed using this approach. Results of assimilation experiments are discussed in the following sections.

4 Observation error formulation

The all-sky assimilation over ocean predicts the total error of FG departures as a function of cloud amount (Geer and Bauer, 2010, 2011). In particular, the observation error is a linear function of the symmetric cloud amount given by the average of observed and simulated polarisation difference at 37 GHz. FG departures are binned according to the symmetric cloud amount and the standard deviations in these bins represent the estimation of the total error. The observation error is then computed from such estimates by removing a small amount representative of background error (1.0 K). To estimate the total error of FG departure over land we followed an equivalent approach, but the scattering index (SI) given by the difference between SSMI/S channel 18 and channel 8 (91h - 150h) has been chosen as symmetric predictor. The use of this SI as a predictor can be considered reasonable for two main reasons: a) at higher microwave frequencies over land surfaces the use of scattering signal to identify precipitation and convective areas has been investigated in literature by many authors (i.e. Bennartz and Bauer 2003, Bennartz et al., 2002, Sun and Weng 2012); b) previous studies on the possibility of extending all-sky assimilation over land surfaces (Baordo et al., 2012) showed the beneficial use of the observed scattering index to discriminate moderate and intense scattering regions.

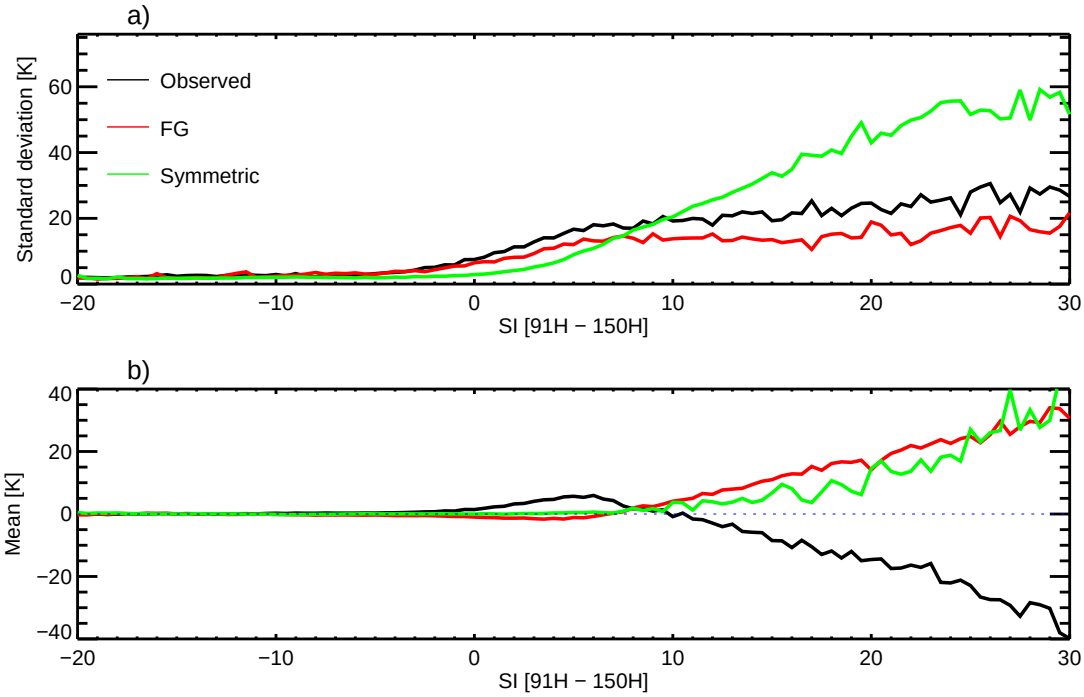

Figure 3: Standard deviation (a) and mean (b) of SSMI/S channel 183±7 FG departures for the month of June 2012, binned as a function of observed scattering index (black), FG scattering index (red) or symmetric scatting index (green). Statistics are for those observations over land between 60°S and 60°N. Bin size is 0.5 K.

Figure 3 shows standard deviation (a) and mean (b) of SSMI/S channel 183±7 FG departures, binned as a function of observed scattering index (SI^{obs}), FG scattering index (SI^{FG}) or symmetric scattering index (SI^{sym} = [SI^{obs} + SI^{FG}]/2). Figure 3b encapsulates the 'mislocation error' issue: there are situations where there is more snow in the observations than in the model (hence negative FG departure biases) counterbalanced by cases where observations are clear and forecast model is simulating more snow than is observed or radiative transfer calculation is simulating excessive scattering (hence positive FG departures biases). Binning by SI^{sym} still reveals biases which are roughly constant between scattering index values of 10 K and 20 K, and increase for SI^{sym} greater than 20 K, reaching values larger than +30 K. However, about 95% of the total number of observations are within the region where binning by SI^{sym} does not show biases ($SI^{sym} < 10$ K), and the remaining 4% and 1% of data are distributed, respectively, where 10 K $< SI^{sym} <$ 20 K and $SI^{sym} > 20$ K. Additionally, means of 183±3 and 183±1 FG departures binned as a function of the symmetric scattering index (equivalent of Figure 3 not shown here) do not reveal biases for $SI^{sym} < 20$ K. As a conclusion, we can infer that the scattering index is a good predictor to estimate the total error of FG departure. We chose to reject observations wherever SI^{sym} is greater than 20 K resulting in loss of only 1% of data, although the safest case of assimilating observations only if SI^{sym} is less than 10 K has been also investigated.

It is worth mentioning that conclusions derived from Figure 3 would not be possible if Mie sphere approximation was used to perform radiative transfer calculations. In this case, positive FG departures biases would be completely missed, a result equivalent to that of Figure 1, where the histogram of FG departures is asymmetric with no tail of positive departures.

We can now use the standard deviation of SSMI/S channels FG departures, binned as a function of

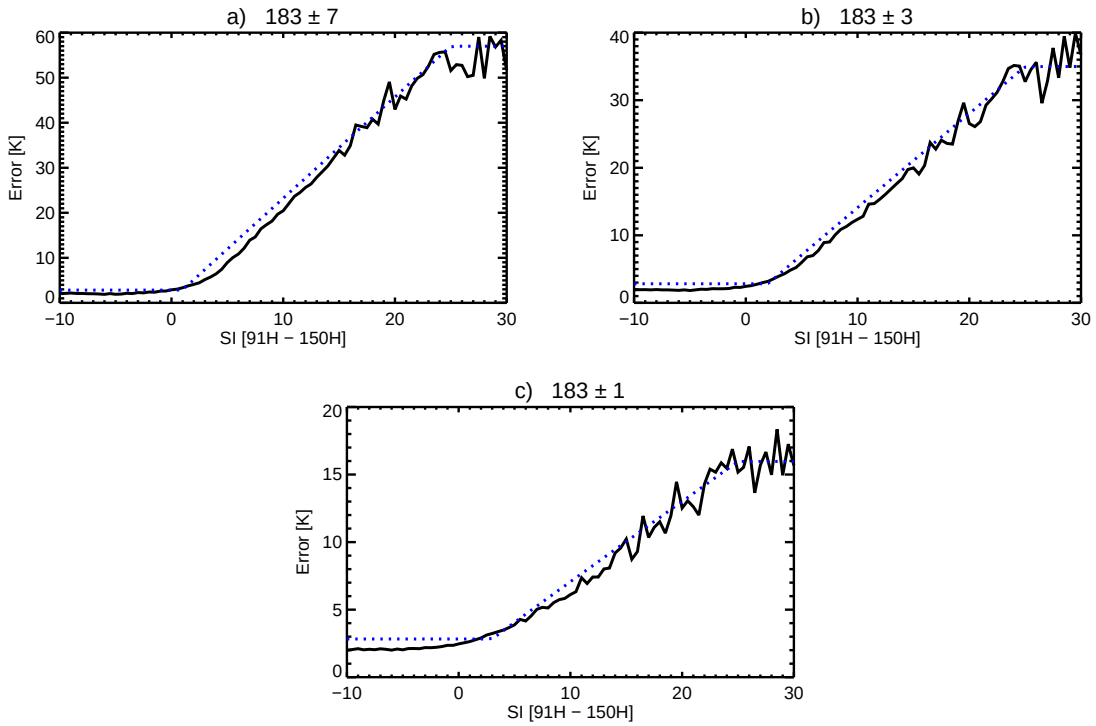

Figure 4: Error model for SSMI/S humidity sounding channels, showing how the standard deviations of FG departures binned as a function of symmetric scatting index (black solid line, equivalent of Figure 3a) are modelled by a linear fit (blue dashed line).

SI^{sym} (equivalent of Figure 3a) to estimate the total observation error. Figure 4 shows how the standard deviations of SSMI/S humidity sounding channels FG departures have been modelled in order to have an observation error formulation. Three areas can be identified as follows:

1. region a: where standard deviations of FG departures are constant;
2. region b: where standard deviations of FG departures can be linearly fitted;
3. region c: where standard deviations of FG departures seem to stop increasing.

Region a can be interpreted as the clear-sky area where observations are unaffected by scattering and presumably free of clouds and precipitation. For every SSMI/S sounding channel this area has been graphically estimated according to SI^{sym} values ('clear-sky thresholds'): $SI^{sym} < 1$ K for 183±7, $SI^{sym} < 2$ K for 183±3, $SI^{sym} < 3$ K for 183±1. The clear-sky total observation error for every SSMI/S humidity sounding channel has been assigned constant and equal to 3 K. This error is quite comparable to the observation error used for the equivalent MHS channels which are assimilated in clear-sky conditions and have a 2 K error assigned. Region b, instead, is where the influence of scattering, cloud and precipitation on observations increases, as well as the standard deviations of FG departures. This trend seems to be well approximated by a straight line and, as a consequence, the observation error in this area can be derived by a linear fit starting from the clear-sky threshold to SI^{sym} value of 25 K. The latter value has been graphically evaluated as the starting point of the region c, where the linear behaviour of the standard deviations of FG departures seems to be lost. This is an approximation that might be rough, but considering that any observation where $SI^{sym} > 20$ K will be discarded, the assimilation will not be affected. The all-sky maximum observation error (corresponding to SI^{sym} value equal or greater than 25 K) has been estimated as 57 K for 183±7, 35 K for 183±3 and 16 K for 183±1.

The reliability of the observation error formulation is explored through Figures 5, 6 and 7. Figure 5 shows maps of mean observation errors for SSMI/S humidity sounding channels for the month of June 2012 and map of total hydrometeor content given by the sum of model first guess cloud, rain, snow and ice water path. Observations have been selected according to the equivalent MHS screening (hereafter mentioned as MHS-like screening) that is currently used operationally at ECMWF (use of different surface screening is investigated within assimilation experiments and is discussed in section 6). MHS-like screening uses surface temperature and orography thresholds (according to the channel sensitivity to the surface) to reject observations. Observations are discarded if:

- model surface temperature is less than 278 K;
- model orography is greater than 1500 m, 1000 m or 800 m, respectively at 183±7, 183±3 and 183±1.

White spots in Figure 5a, 5b and 5c indicate regions where such screening is applied. Considering the map of mean total hydrometeor content as an indicator of model cloudiness (5d), we can infer that smallest and largest observation errors are localised, respectively, in area of low (clear-sky regions) and high (cloudy-sky regions) total hydrometeor content amount.

Figure 6 checks the effectiveness of SSMI/S humidity sounding errors comparing normalised departures (normalised departure is the FG guess departure divided by the total error predicted by the symmetric error model) over land with those over ocean within an assimilation experiment where 183 GHz channels are assimilated over both land and ocean. The model error distribution over land produces normalised departures that are quite small suggesting that error estimates might be a bit large. However, as for the ocean case, this condition is not necessarily a bad thing. The overall result of such 'safe' error estimation is mainly to give less weight to these observations. This limitation might be overcome by

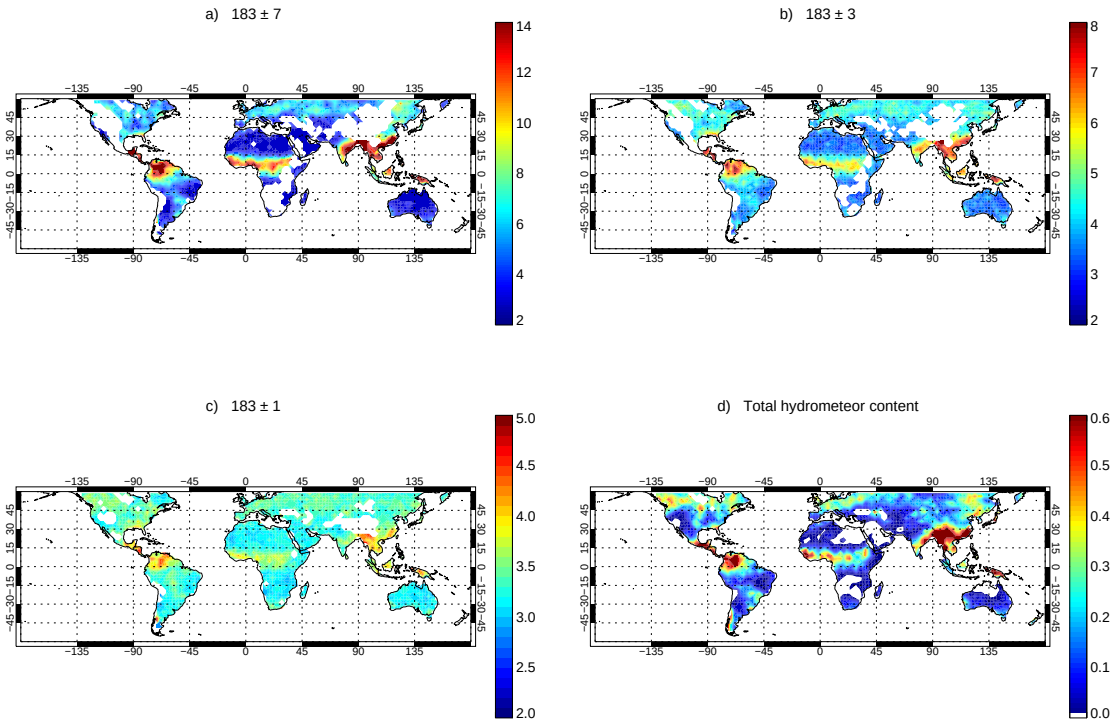

Figure 5: Maps of mean observation errors [K] for SSMI/S humidity sounding channels (a, b, c) and total hydrometeor content [kg/m^2] given by the sum of model first guess cloud, rain, snow and ice water path (d), for the month of June 2012. White spots in maps a, b, c identify regions where the surface temperature and orography screening are applied. Means are computed in bins of 2.5° by 2.5° in latitude and longitude.

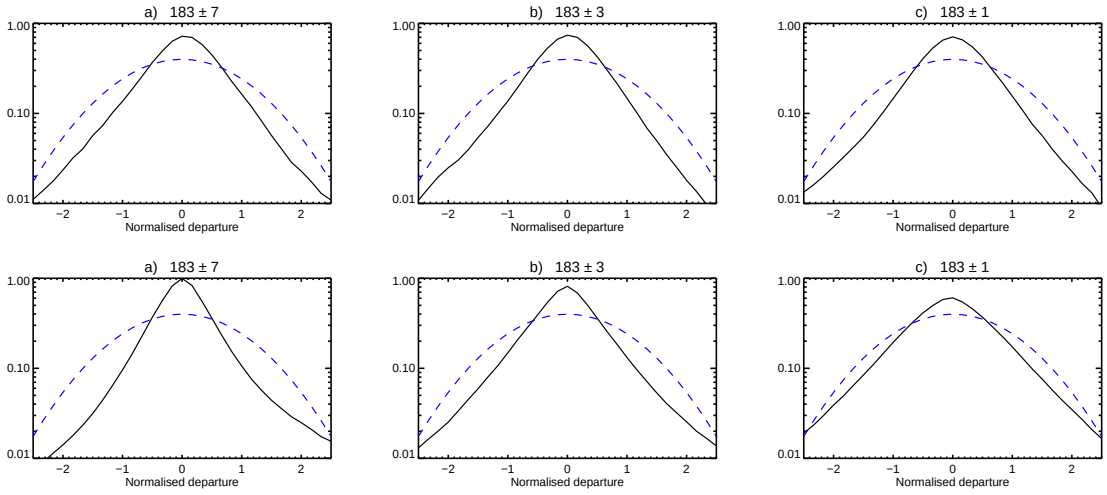

Figure 6: Log histograms of normalised SSMI/S humidity sounding FG departure (blakc solid line) for the month of June 2012: all-sky observations over land, top row, and over ocean, bottom row. The dashed line shows a Gaussian with a standard deviation of 1. Sample of observations is between 60°S and 60°N. Bin size is 1.

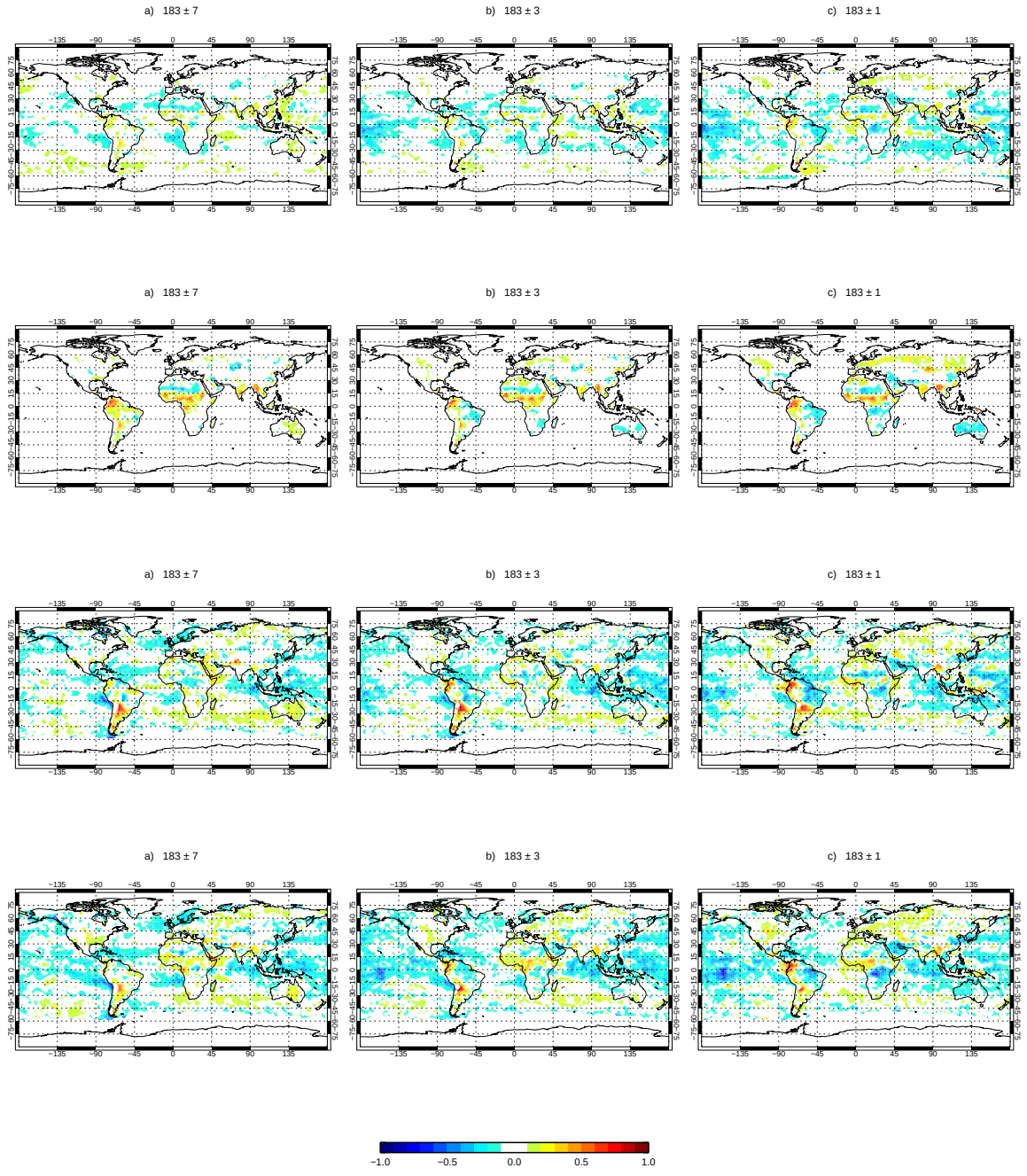

Figure 7: Maps of mean normalised FG departure (after bias correction) for assimilated humidity sounding observations for the month of June 2012. First row: SSMI/S (F17) all-sky assimilation (ocean and land); Second row: SSMI/S (F17) cloud screening and constant observation error assimilation (land only); Third row: NOAA 18 clear-sky assimilation (ocean and land); Fourth row: as third row, but for Metop-A. Means are computed in bins of 2.5° by 2.5° in latitude and longitude.

using a different predictor and, in the future, additional investigations should be carried out. However, considering the reasonable match between ocean and land provided by Figure 6 and taking into account that the all-sky assimilation over land is a new framework to explore, this error model is sufficient to perform assimilation experiments and investigate the impact within the ECMWF system. It is also worth mentioning that an error model based on standard deviation of FG departures depends strictly on the radiative transfer calculation assumptions (i.e. particle's shape and size distribution, surface emissivity etc.): for instance a change of snow particle shape from Mie sphere to DDA sector implies an observation error retuning. The observation error model described in Figure 4 has been derived using DDA sector and 'Cmax' approach and surface emissivity retrieved from observations (in next section more details on surface emissivity are given). It is also important to consider only the sample of observations which will be active in the assimilation and hence to discard data according to the surface screening which is used in the experiment. The error model in Figure 4 has been built considering humidity sounding observations selected according to the MHS-like screening. Different assimilation experiment configurations adopted in this study (i.e different surface screening or use of 'Cav' approach rather than 'Cmax') use different observation error models, slightly re-tuned according to the FG departures for that configuration, but always using same scattering index as predictor.

A second way to evaluate the effectiveness of the observation error model is to look at the size of FG departure biases within assimilation experiments. Considering the high variability of observation errors for SSMI/S (i.e. Figure 5), it is better to examine biases in normalised FG departures than absolute brightness temperatures. In this evaluation we also want to analyse differences between the all-sky and clear-sky assimilation. In particular, the clear-sky assimilation is operationally implemented within the ECMWF system for MHS humidity sounding channels. To identify cloud contamination, MHS observations are discriminated according to FG departure check in the 150 GHz channel. A threshold is applied to the absolute difference between observations and simulated clear-sky radiances: observations are part of the 4D-Var minimisation only if the difference is less than 5 K. For a fairer comparison, we run an experiment in which SSMI/S humidity sounding channels over land were assimilated using the MHS cloud detection and assigning same constant observation error of 2 K. This experimentation still uses in the all-sky framework (i.e. DDA sector and 'Cmax' to compute radiative transfer calculations), but, by means of the cloud screening, we can evaluate the impact on the system of removing radiances affected by cloud and precipitation. To also have equivalent observation coverage, SSMI/S data were assimilated using the same surface screening criteria (orography and surface temperature checks as mentioned before).

Figure 7 evaluates the all-sky assimilation impact, comparing, for the month of June 2012, normalised FG departures for assimilated SSMI/S humidity sounding observations to the equivalent assimilated MHS observations from NOAA 18 and Metop-A: first row is for SSMI/S data assimilated in the all-sky approach (over both ocean and land); second row is for SSMI/S observations over land when the cloud screening and constant observation error are applied; third and fourth rows are, respectively, for the clear-sky assimilation of NOAA 18 and Metop-A (over both ocean and land).

The overall result is that the all-sky approach over land brings normalised biases as small as over ocean (first row), confirming the consistency of the observation error formulation and in general, the assimilation strategy itself. Clear-sky and 'cloud screening' assimilation, instead, shows regions over Southern America and Central Africa in which biases are slightly larger than in other areas. It is important to point out that the SSMI/S 'cloud screening' assimilation over land (second row) implements, as already mentioned, the use of DDA sector and 'Cmax' approach: possible remaining cloud contamination might bring colder simulated brightness temperatures due to more scattering from snow hydrometeors and as a consequence larger positive FG departures. This might be the explanation of the larger positive FG

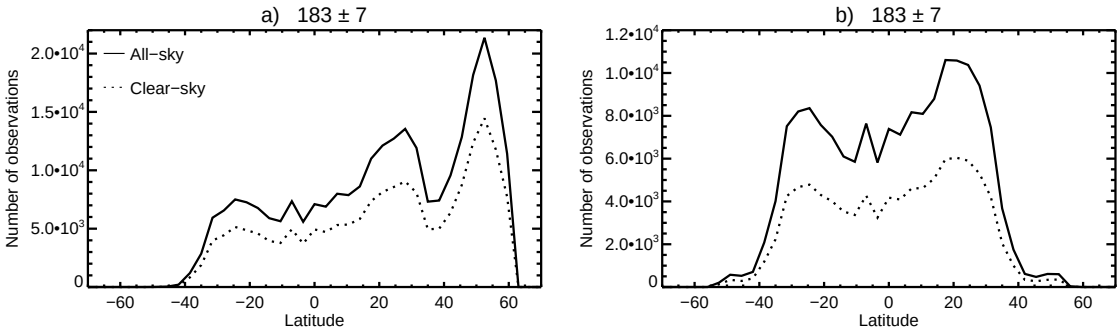

Figure 8: Number of observations in 3.5° latitude bins for the month of June (a) and January (b) 2012 using either all-sky (black line) or clear-sky (dotted line) approach when the MHS-like surface screening is applied to SSMI/S channel 9 (183±7 GHz).

SSMI/S channel	19h	19v	37h	37v	91h	91v
Brightness Temperature [K]	285.32	283.42	268.81	269.18	222.67	225.66
Emissivity retrieved	0.947	0.944	0.881	0.884	0.284	0.357
Emissivity from TELSEM	0.966	0.971	0.954	0.959	0.951	0.956

Table 2: Cloud contamination impact on emissivity retrievals obtained using SSMI/S observations over land. Set of observations are for 1st June 2012, over the North-East of China near the Russian border.

departures over Central Africa for SSMI/S compare to NOAA 18 and Metop-A assimilation. In this comparison, we also have to take into account the different geometry and sensitivity of the instruments as well as possible small biases in surface emissivity estimations. However, we can generally conclude that SSMI/S, NOAA 18 and Metop-A clear-sky assimilation, independently of the sensor, bring roughly the same result. Similar results are seen for January 2012 (not shown).

The difference between all-sky and cloud screening assimilation can be also evaluated in terms of observation coverage. Figure 8 compares coverage as a function of latitude for the month of June and January 2012, for SSMI/S observations in the all-sky and clear-sky approaches. Observations are also screened out according to the MHS-like surface screening. In regions where the surface screening does not cut the most of the observations, Figure 8 shows that the all-sky brings about two times more data than the cloud screening case.

5 Surface emissivity

Land surface emissivity estimates can be obtained using satellite observations, a method commonly adopted in literature (i.e. Prigent et al. 2005). In the all-sky approach, the implementation of the emissivity retrieval from satellite data was coded within the scattering radiative transfer code so that the emissivity estimate takes into account cloud and precipitation. The technical implementation and feasibility of the emissivity retrieval embedded within the all-sky framework has already been evaluated by Baordo et al. (2012). In this section, we discuss the criteria that has been chosen to keep or reject the resultant emissivity estimation, and, hence, what the sample of land surface emissivities used to compute radiative transfer calculations looks like (hereafter mentioned as sample of FG emissivities).

The study carried out by Baordo et al. (2012) pointed out that cloud contamination is the main issue to

take into account when emissivity retrievals are computed using satellite observations. Table 2, comparing emissivity estimates obtained from SSMI/S window channels (horizontal and vertical polarisations) to those provided by TELSEM, encapsulates the nature of this problem. SSMI/S observations in Table 2 are for a geographical location (North-East of China near the Russian border) not affected by critical orography or surface temperature conditions: orography is less than 500 meters and surface temperature is 295 K. Emissivity retrieval deficiencies depend on cloud contamination which affects observed brightness temperatures and as a result brings unreliable emissivity estimates. Moving from 19 to 91 GHz, the higher is the microwave frequency, the larger is the depression in the radiances: channels at 37 GHz and 91 GHz are, respectively, 15-20 K and about 60 K colder than those at 19 GHz. Cloud contamination is not an issue for low frequencies and, hence, 19 GHz channels bring realistic emissivity estimates, similar to those provided by TELSEM for the equivalent geographical location. Emissivity retrievals at higher frequencies (37 GHz) begin to be affected by cloud contamination and the resultant emissivity estimations are slightly lower than TELSEM, but they still might be considered reasonable (for instance, cloud and precipitation might produce changes in surface conditions such as soil moisture or temperature). Channels at 91 GHz, instead, are those mostly affected by cloud contamination and as a consequence the resultant emissivity retrievals are completely unrealistic.

In our all-sky assimilation approach, we want to retrieve emissivities in window channels (those of Table 2) and then reassign these estimations to higher frequencies, according to the right polarisation, in order to perform radiative transfer calculations. For instance, emissivities retrieved at 19h, 37h and 91h are used for radiative transfer calculations, respectively, at 37h, 91h and 150h and humidity sounding channels. In order to limit the influence of cloud contamination on the emissivity retrieval at any frequency, we investigated cases such as those of Table 2 for the month of June and January 2012. We found that observed SSMI/S radiance difference at channel 12 and channel 18 (19h - 91h) is a good way to discriminate cloud contamination within emissivity retrievals. If the difference of observed brightness temperatures (19h - 91h) is less than 20 K, the observation is used to retrieve emissivity; otherwise it is rejected. Using this approach, for both June and January, the sample of retrieved emissivities has been assessed by comparison with the equivalent sample of emissivity estimations provided by TELSEM. Table 3, for every SSMI/S window frequency for the month of June 2012, compares mean and standard deviation of each sample (retrieved versus TELSEM) and also shows mean and standard deviation of the differences between the two samples (retrieved minus TELSEM). The statistics in Table 3 confirm the good match between SSMI/S window channels emissivity retrievals and TELSEM estimations. Similar statistics are obtained for the month of January (not shown here). Considering these positive results, we used the standard deviation of emissivity differences (retrieved minus TELSEM) as a reference value to guide our choice of keeping or rejecting the emissivity retrieval. The criteria adopted to check the consistency of the emissivity retrieval is as follows:

if abs($\varepsilon_{retrieved}$-ε_{TELSEM}) $< \sigma_v$, retrieval is kept, otherwise estimate from TELSEM is used.

The threshold σ_v is different for every SSMI/S window channel and has been estimated as roughly two times the standard deviation of emissivity differences (retrieved minus TELSEM) of Table 3: 0.04 (19h), 0.03 (19v), 0.04 (37h), 0.03 (37v), 0.09 (91h), 0.07 (91v). These thresholds have also been identified considering the equivalent statistics of Table 3 for the month of January. The use of this method might be questionable, but, from one side, it can be considered reliable because it is based on monthly statistics, and, on the other side, it tries to compensate the high variability of the land surface emissivity exploiting satellite observations wherever is possible.

The criteria described above was selected to build the sample of FG emissivities which has been used

Channel	19h	19v	37h	37v	91h	91v
Mean of retrieved	0.911	0.959	0.904	0.9514	0.885	0.936
Mean of TELSEM	0.912	0.958	0.905	0.942	0.907	0.935
Stdev of retrieved	0.046	0.020	0.043	0.021	0.058	0.042
Stdev of TELSEM	0.045	0.018	0.041	0.018	0.039	0.021
Mean of differences (retrieved-TELSEM)	0.015	0.011	0.015	0.014	0.030	0.020
Stdev of differences (retrieved-TELSEM)	0.016	0.011	0.018	0.012	0.045	0.034

Table 3: Sample of retrieved emissivities compared to TELSEM for the month of June 2012, wherever observed SSMI/S radiances difference at channel 12 and channel 18 (19h - 91h) is less than 20 K. Statistics are for SSMI/S observations over land between 60°S and 60°N.

to investigate the all-sky assimilation of SSMI/S humidity sounding channels over land. Results of assimilation experiments are described in the next section.

As a reference, when this method is applied to SSMI/S channel 18 (91h), for the month of June, we obtain a sample of FG emissivities consisting of 88% of retrieved and 12% of TELSEM estimates, whilst, for the month of January, the split changes to 82% and 18%. This is reasonable considering that greater cloud contamination in the Northern hemisphere during winter might produce more unrealistic estimates. FG emissivities at 91h are important for the aim of this study since they are used to compute radiative transfer calculations for 150h and humidity sounding channels. In order to analyse in more detail the sample of FG emissivities at 91h, Figure 9 shows maps of mean emissivity differences with the equivalent estimations from TELSEM for the month of June 2012. To explore the sensitivity to the surface, we also split the sample of FG emissivities according to the RTTOV values of the clear sub-column surface to space transmittance (hereafter simply mentioned as transmittance or τ): τ greater and smaller than 0.5 should help to identify, respectively, observations more and less sensitive to the surface. The global emissivity biases (Figure 9a) are driven by 88% of FG emissivities which are characterised by transmittance greater than 0.5 (Figure 9b). The biases observed globally suggest that FG emissivities have on average values 0.02-0.04 smaller than TELSEM estimations. The remaining 12% of FG emissivities (τ less than 0.5, Figure 9c) is also affected by same biases.

Another way to view at the reliability of FG emissivities is shown in Figure 10, where histogram of FG emissivities are compared to TELSEM for the month of June. Comparisons are again made for different transmittance values (greater and less than 0.5). Empty bins have been assigned the value 0.1 to better distinguish occurrences from TELSEM and retrievals. The general outcome is that the distribution of FG emissivities fits quite well that of TELSEM estimates. We can additionally identify: a) those emissivity retrievals (between 0.5 and 0.7) which are missing in the TELSEM data set (i.e. black cross only); b) those emissivity values (less than 0.5 and between 0.5 and 0.6) which come from TELSEM and where the retrievals have been rejected due to being too different from TELSEM (i.e. perfect overlap between black cross and red diamond). It is worth mentioning that similar conclusions can be drawn for the month of January.

6 Assimilation experiments

6.1 Summary

To explore the impact on analyses and forecasts of assimilating SSMI/S 183 GHz channels over land in the all-sky approach, a number of experiments were run at cycle 38r2. In order to take into account

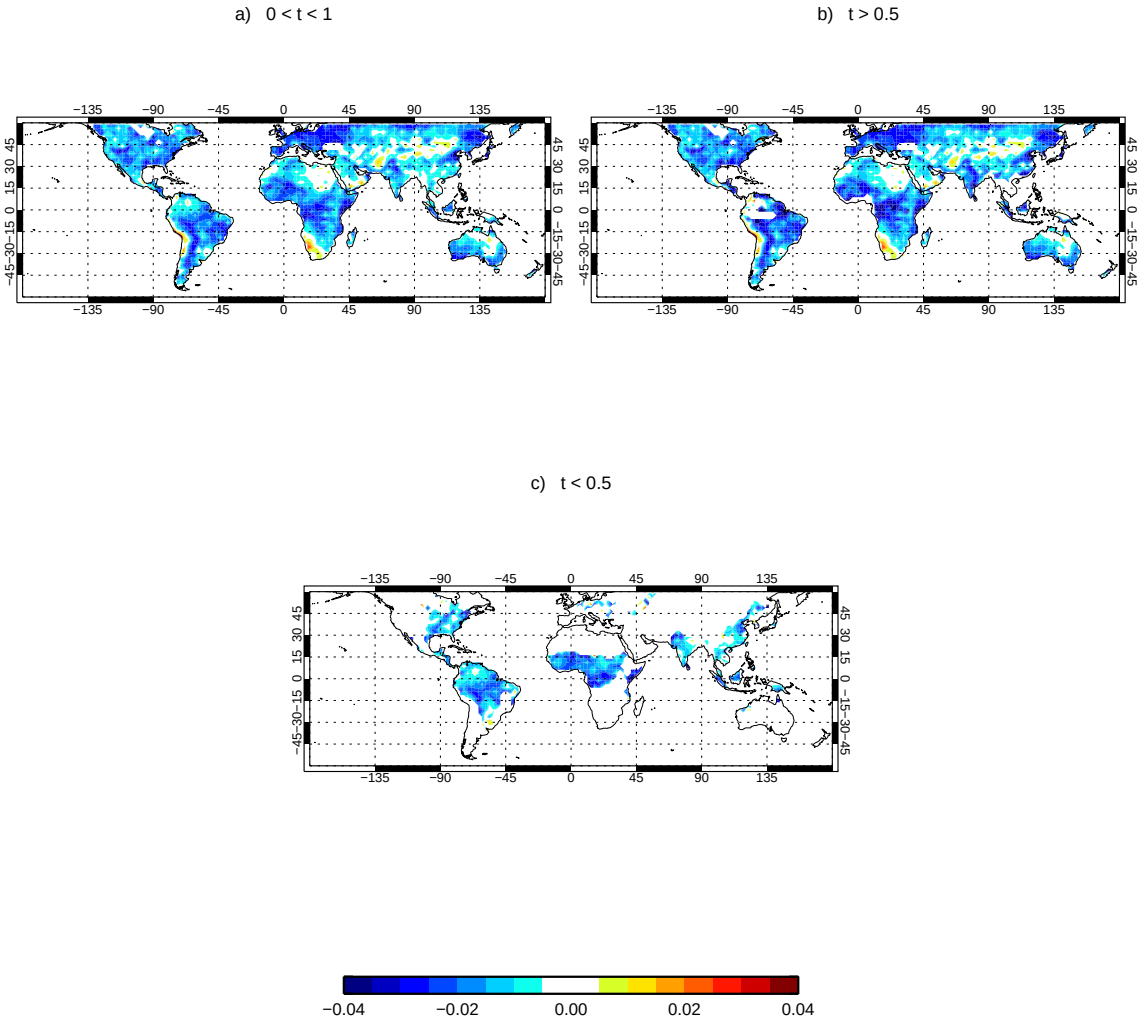

Figure 9: Maps of mean emissivity differences (FG - TELSEM) at 91h for the month of June 2012. Sample of FG emissivities is obtained from observations over land between 60°S and 60°N (a) and split according to transmittance values: b) τ greater than 0.5, and, c) τ less than 0.5. Means are computed in bins of 2.5° by 2.5° in latitude and longitude.

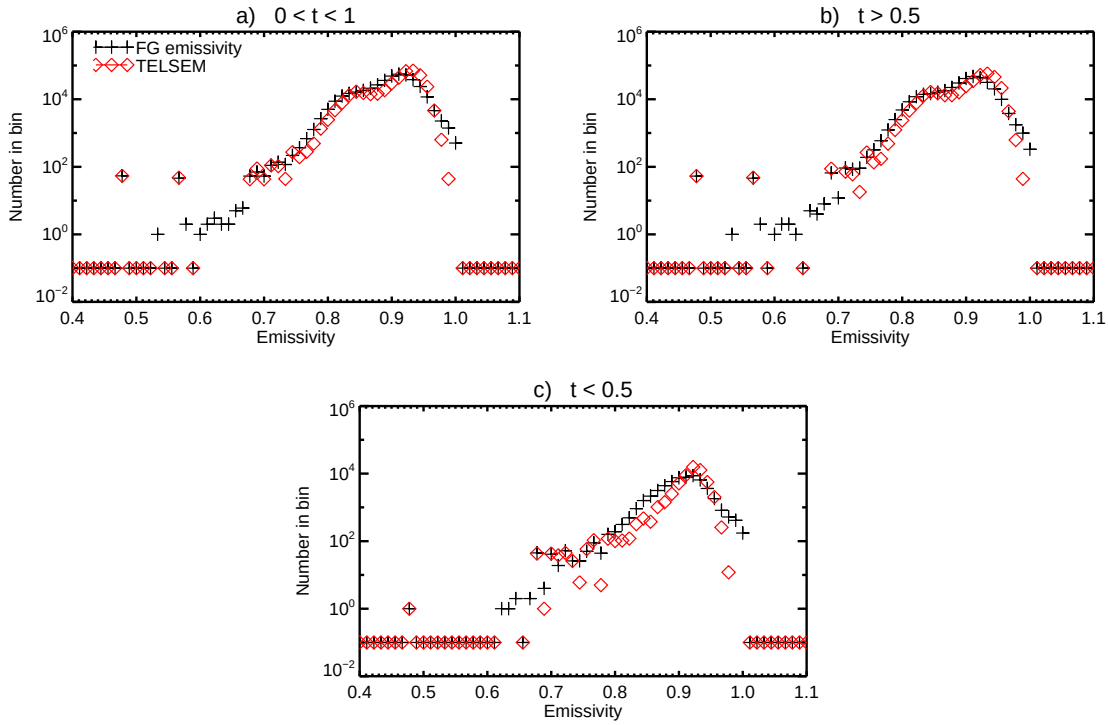

Figure 10: Histogram of FG emissivity (black cross) at 91h compared to TELSEM (red diamond) for the month of June 2012. Sample of FG emissivities is obtained from observations over land between 60°S and 60°N (a) and split according transmittance (τ) values: b) τ greater than 0.5, and, c) τ less than 0.5. Bin size is 0.01. Empty bins have been assigned the value 0.1 (10^{-1} in figure) to better distinguish occurrences from TELSEM and retrievals.

the important all-sky developments over ocean, our control experiment includes the changes of the all-sky over ocean package (Geer 2013). The latter contains important modifications such as: use of DDA sector to model radiative transfer calculations for snow hydrometeors; retuning of observation errors; active assimilation of SSMI/S 183 GHz channels. In this way, outcomes from any all-sky assimilation experiment over land can be evaluated as the result produced on top of the entire all-sky package over ocean which will be supplied for cycle 40r1. Control and assimilation experiments of SSMI/S 183 GHz channels over land were run at T511 horizontal resolution and 137 vertical levels in a 4D-Var 12 hour assimilation window. In the following sections, a detailed description of the experimentation carried out within the ECMWF assimilation system is provided.

6.2 All-sky assimilation impact

In order to justify an eventual introduction of the all-sky assimilation over land within the next available IFS cycle (i.e. 40r2), we have to explore the reliability of the framework within the system from both a technical and scientific point of view. Technically, the developments must be efficiently coded and guarantee the functionality of the system as before. This is implicitly done during the implementation of the framework. Scientifically, the advantages that the assimilation system might have must be demonstrated through analysis and forecast verifications.

Experimentation, which covers 3 months of period (June to August 2012), to evaluate the impact of the all-sky assimilation over land can be summarised as follows:

- Control experiment: 38r2 all-sky over ocean package + SSMI/S observations over land introduced passively into the system.
- Experiment 1, all-sky assimilation: as Control, but SSMI/S 183 GHz channels actively assimilated over land using the all-sky developments: radiative transfer calculations upgrade (DDA sector and ‘Cmax’ approach) + surface emissivity retrieval + observation error formulation.
- Experiment 2, cloud screening assimilation: as Control, but SSMI/S 183 GHz channels actively assimilated over land using: radiative transfer calculations upgrade (DDA sector and ‘Cmax’ approach) + surface emissivity retrieval + cloud contamination check (150 GHz) + constant observation error (2 K).

Both experiment 1 and experiment 2, as already explained in section 4, reject observations if the symmetric scattering index is greater than 20 K. They also implement the surface screening based on temperature and orography thresholds. Observations are rejected if (as already mentioned in section 4):

a. model surface temperature is less than 278 K;

b. model orography is greater than 1500 m, 1000 m or 800 m, respectively at 183$\pm$7, 183$\pm$3 and 183$\pm$1 GHz.

Experiment 2 is not the equivalent clear-sky assimilation operationally used for MHS data which implements no scattering radiative transfer calculations. However, it is still a valid reference to evaluate the impact on the system of removing radiances affected by cloud and precipitation. Thus, we can investigate if cloud and precipitation affected radiances over land brings more information into the assimilation system.

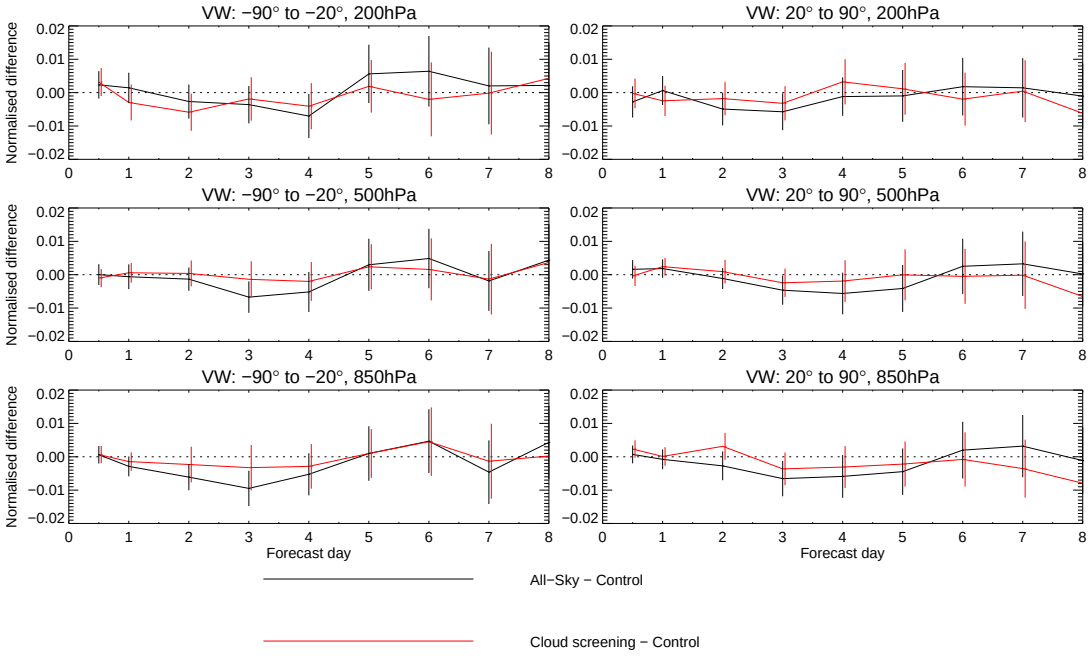

Figure 11: Normalised change in RMS forecast error in vector wind at 200 hPa (top row), 500 hPa (middle row) and 850 hPa (bottom row) for the Southern (-90° to -20°) and Northern (20° to 90°) hemisphere. Verification is against own analysis. Scores are based on a 3 months period, June to August 2012. Error bars indicate the 95% confidence level.

Differences between the all-sky and the cloud screening assimilation are investigated through Figure 11, 12 and 13 which show normalised change in RMS forecast error for vector wind, relative humidity and geopotential height at 200 hPa, 500 hPa and 850 hPa for the Southern (-90° to -20°) and Northern (20° to 90°) hemisphere. Verification is against own analysis and scores are based on 3 months period (June to August 2012). Both the all-sky and the clear-sky experiment are compared to the control experiment ('Experiment minus Control') and negative values indicate reduce RMS forecast errors, hence an improvement respect to the control. The overall outcome can be summarised as follows:

1. Using the all-sky assimilation, RMS errors in vector wind (Figure 11) are reduced from the lower to the upper part of the troposphere in both the Southern and Northern hemisphere. In particular, RMS errors appear to decrease at shorter ranges and increase, not significantly, at longer ranges (day 6, 7 and 8). Changes are observed at 850 hPa in both the hemispheres: in the Southern hemisphere RMS error reduction of about 1% is observed at day 3 and about 0.5% at day 2 and 4, while in the Northern hemisphere, day 3, 4 and 5 are characterised by a decrease of about 0.5%. There is same trend at 500 hPa, but with slightly smaller RMS error reduction. At 200 hPa in the Southern hemisphere the all-sky assimilation seems to be slightly worse than experiment 2. However, in the Northern hemisphere, the better performance of the all-sky assimilation is again visible from day 2 to day 5.

2. Analysing plots for relative humidity (Figure 12), we can generally conclude that differences between the two experiments are less significant. The all-sky assimilation produces slight better results, with two significant changes observed: a) at 200 hPa in the Southern hemisphere, RMS error reductions of about 1% and 0.5% are respectively observed at day 3 and 4; b) at 500 hPa in

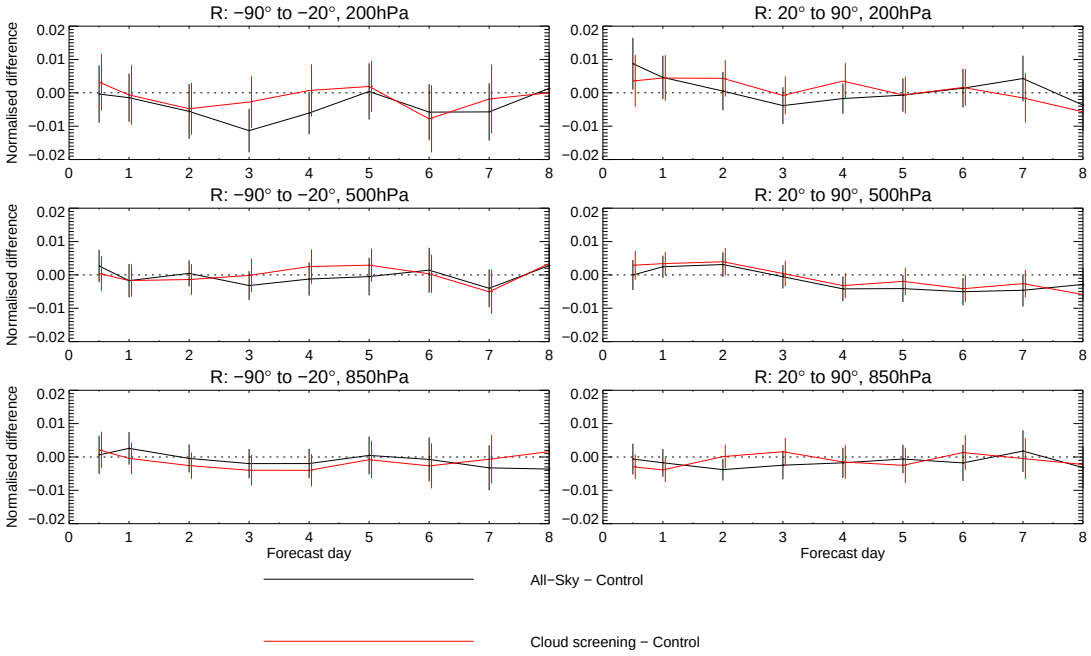

Figure 12: As Figure 11, but showing the normalised change in RMS forecast error in relative humidity.

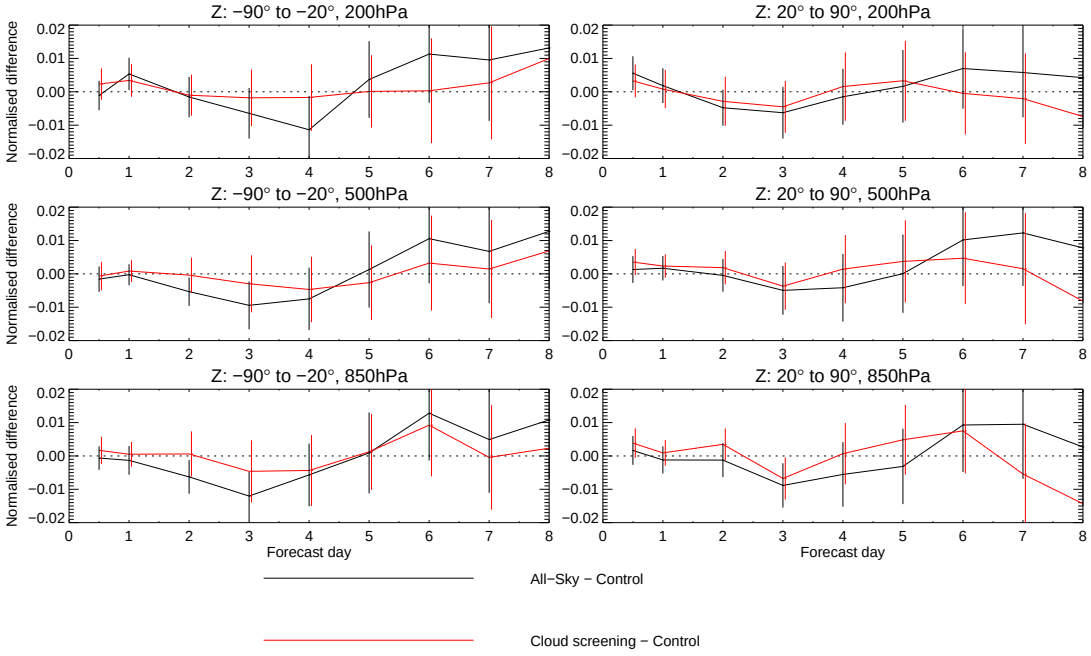

Figure 13: As Figure 11, but showing the normalised change in RMS forecast error in geopotential height.

the Northern hemisphere, decrease in RMS error of about 0.5% is constant from day 4 to day 7. An exception to the better all-sky performance is at 850 hPa in the Southern hemisphere, where the cloud screening assimilation produces slightly better results.

3. Results for geopotential height (Figure 13) are very similar to those of vector wind: both the hemispheres are characterised by smaller and larger RMS errors at shorter and longer ranges respectively. Important significant changes are observed in the Southern hemisphere, at 500 hPa and 850 hPa (day 2, 3 and 4) as well as at 200 hPa (day 3 and 4), and in the Northern hemisphere, at 850 hPa (day 3).

Another general conclusion that can be drawn from this investigation is that the all-sky water-vapour sounding channel assimilation seems to be more effective at improving wind rather than relative humidity scores. This outcome can be explained by two main considerations: a) the assimilation system is already fed with many other microwave humidity sounding observations both over ocean and land (i.e ocean and land data from 3 MHS and ATMS instruments and ocean observations from SSMI/S) and, as a consequence, the humidity analysis and forecast is much more constrained by those observations. For instance, considering only SSMI/S data, 1 month of all-sky assimilation of humidity sounding data (183 ± 7, 183 ± 3 and 183 ± 1 GHz) brings over ocean about 3 million of observations into the system, while over land the assimilated number is roughly four time smaller (about 700 thousand data). b) The impact of water vapour sounding channels on wind fields might be explained by the 4D-Var tracer effect. The feature-tracing of water vapour, cloud and precipitation structures likely leads to a better adjustments of the wind fields and, as a result, also a small number of assimilated cloud affected observations might play an important rule in the wind analysis and forecast.

These considerations can be additionally extended looking at the normalised change in the RMS forecast error of vector wind, plotted zonally (i.e. latitudes versus pressure levels): Figure 14 shows change in the RMS of wind forecast error between the all-sky experiment and the control, while Figure 15 visualises the equivalent for the cloud screening experiment. Comparison of the two plots suggests again that the all-sky assimilation makes the forecast errors smaller. In particular, significant changes can be noticed at day 3 and 4. These improvements are mainly observed in the austral winter at polar latitudes (between 75°S and 60°S). This behaviour is very interesting because the all-sky assimilation over land is only active between 60°S and 60°N. The explanation might be found again in the the 4D-Var water vapour tracing capability linked to the dynamics of the atmosphere. During the austral winter the atmosphere is dynamically very active and, as a consequence, the improved forecasts might be explained by an improved representation of polar tropospheric and upper-tropospheric winds. The all-sky assimilation might bring into the systems new kinds of observations characterised by strong convection over land, improving the analysis of the winds through the troposphere in the Southern hemisphere storm tracks and these improvements might be propagated into the polar regions during the forecast. It is worth pointing out that similar findings showed up when the SSMI/S 183 GHz channels were initially assimilated in the all-sky approach over ocean.

An alternative way to check the impact on winds is to examine for both the all-sky and the cloud screening experiment fits to conventional observations (i.e. TEMP-U and TEMP-V) through the experimentation period. Figure 16 shows the normalised change in standard deviation of analysis departures and FG forecast departures for wind conventional observations (combining TEMP-U and TEMP-V) in the Southern and Northern hemisphere, whilst in Figure 17, fits to AMVs in the Antarctic area are analysed. Results indicate that standard deviation of FG forecast departures, when the assimilation is carried out in the all-sky approach, are generally reduced compare to the control and smaller compared to the case when the cloud screening assimilation is used. Fits to TEMP-U and TEMP-V observations indicate that

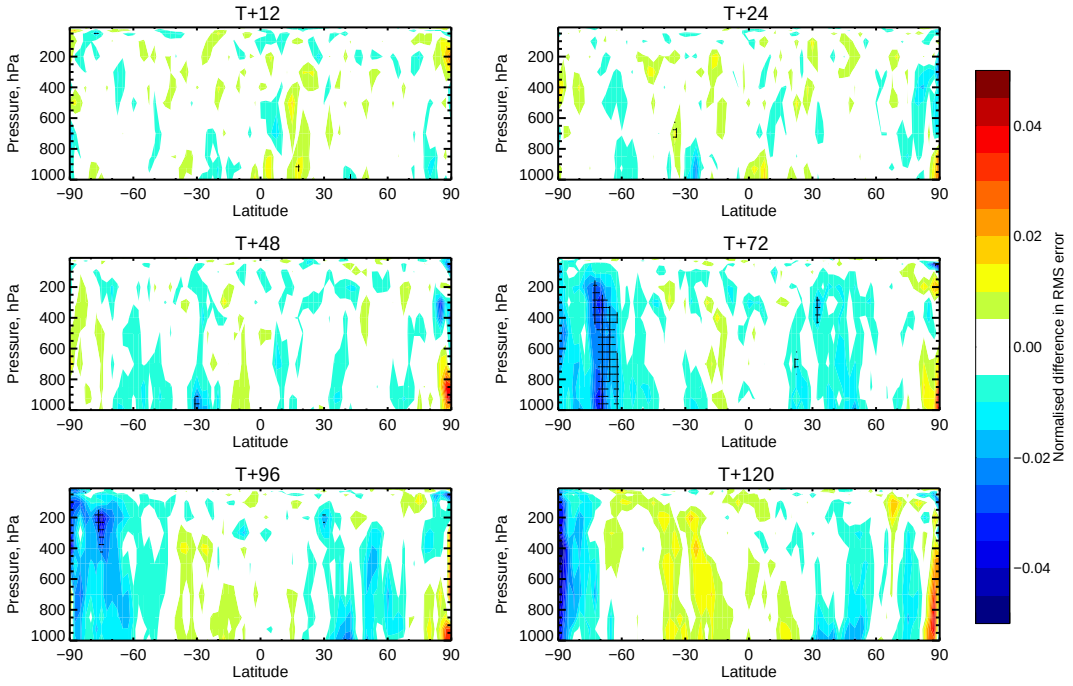

Figure 14: Normalised change in the RMS of vector wind forecast error between the all-sky experiment and the control. Verification is against own analysis and score are based on a 3 months period, June to August 2012. Negative values (light and dark blue areas) show reduced RMS forecast errors; cross-hatched areas indicate a statistically significant change with 95% confidence level.

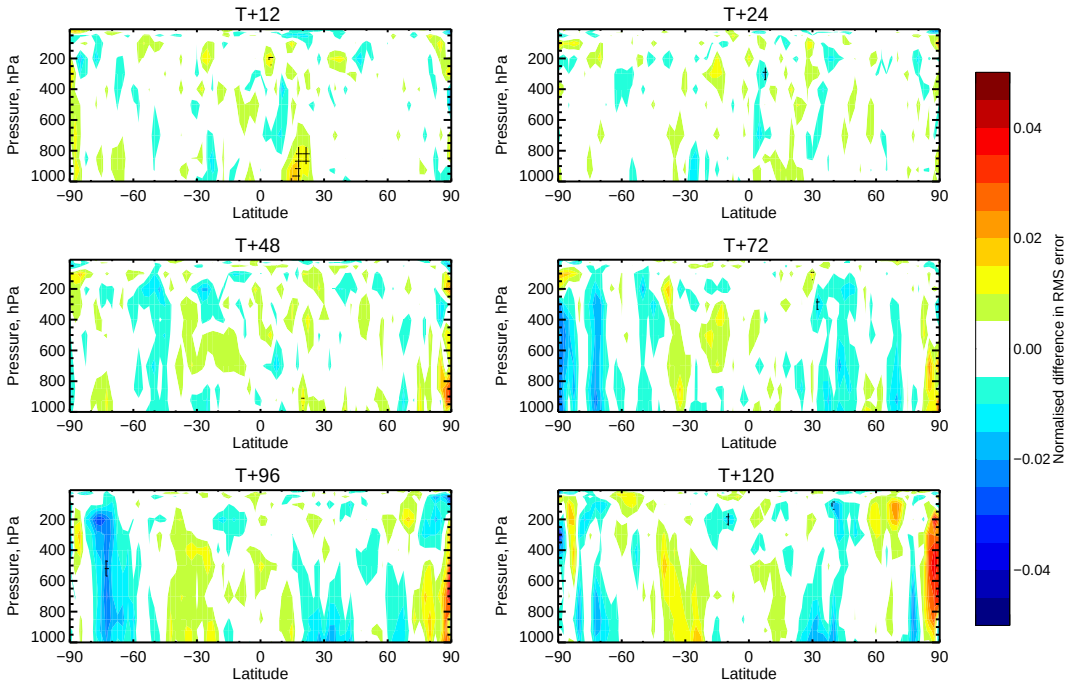

Figure 15: As Figure 14, but showing the normalised change in the RMS of vector wind forecast error between the cloud screening experiment and the control.

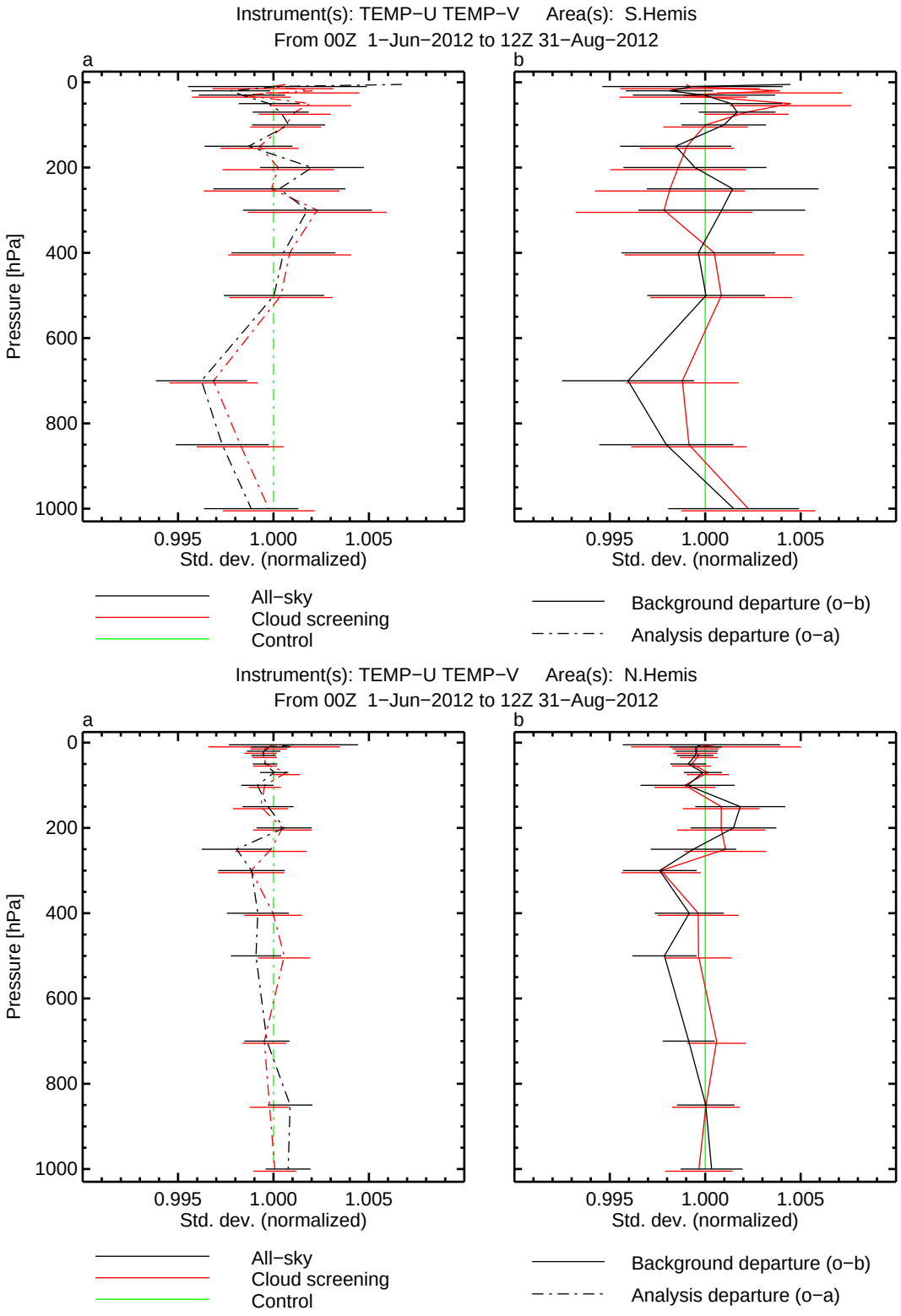

Figure 16: Normalised change in standard deviation of analysis departures (left) and FG forecast departures (right) for wind observations (TEMP-U and TEMP-V).Top row and bottom row show, respectively, fits for the Southern and the Northern hemisphere. Standard deviations are normalised by those of the control experiment. Error bars indicate the 95% confidence level. Statistics are for 3 months of period (June to August 2012).

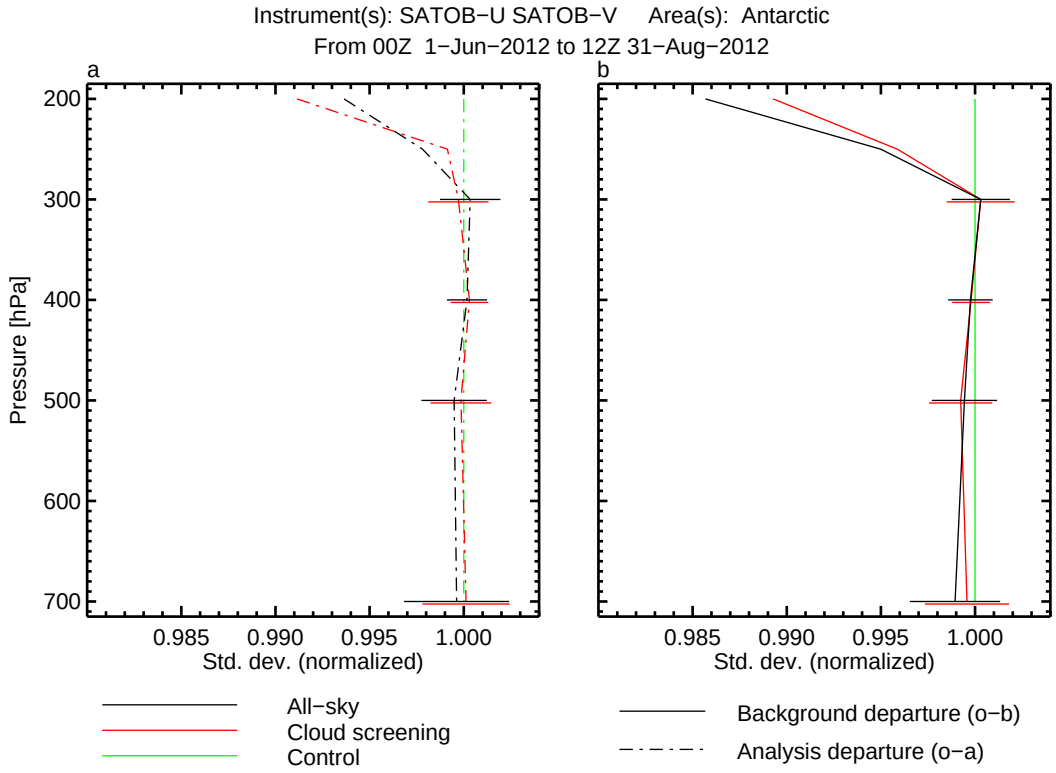

Figure 17: As Figure 16, but for AMVs in the Antarctic area.

the all-sky approach brings statistically significant reductions of about 0.4% at 700 hPa in the Southern hemisphere and about 0.2% at 500 hPa in the Northern hemisphere. Exception to this trend is between 300 and 200 hPa in the Southern hemisphere, where the cloud screening assimilation produces smaller standard deviations. However, at the same pressure levels, in the Antarctic, fits to AMVs observations show that the all-sky assimilation produces better improvements reaching a significant change of about 1.4% at 200 hPa. This might be an additional verification of the link between the all-sky assimilation and the 4D-Var tracing effect.

The general conclusion of this section is that the all-sky assimilation of humidity sounding channels over land brings new useful information into the system benefiting, in particular, winds analysis and forecasts. In the next section, we discuss results from other assimilation experiments in order to additionally demonstrate the reliability of the all-sky approach over land.

6.3 Reliability of the all-sky assimilation over land

Conclusions drawn in the previous section are in favour of the all-sky assimilation over land, even though it would be good to have further indication of the reliability of the all-sky approach. In order to achieve this goal, we additionally compare the results of the all-sky assimilation to those provided by two other experiments which are characterised by same configuration of the all-sky experiment, but with smaller number of assimilated observations. A ‘safer’ assimilation experiment with more data rejected will help to identify which observations have more impact on the assimilation system. In general, through this approach, we might understand whether we are improving or deteriorating the system and which

beneficial information we are supplying.

To make statistics more significant, experimentation was extended considering 3 additional months, covering also the winter period (January to March 2012). The two other experiments are characterised by the following changes:

- Experiment 1: same configuration of the all-sky experiment (described in previous section and in the following text mentioned as 'standard' all-sky to avoid confusion), but rejecting all observations wherever the symmetric scattering index is greater than 10 K (threshold for the all-sky experiment is 20 K). In the following this experiment is also mentioned as all-sky(SI10).
- Experiment 2: same configuration of the all-sky(SI10), but SSMI/S channel 9 (183±7 GHz) is also blacklisted. Hereafter this experiment is also named as all-sky(SI10 ch9 denied).

The all-sky(SI10) experiment helps to understand the impact of observations affected by larger scattering index values. These observations are localised in cloudy, precipitating or convective areas. The all-sky(SI10 ch9 denied) experiment not only implements the conservative scattering index screening, but also rejects all observations at 183±7 GHz. SSMI/S channel 9, which among the humidity sounding channels is the most sensitive to lower part of the troposphere, so this experiment investigates the impact on the system of assimilating those observations which might be affected by surface conditions. Results of the experimentation are summarised below.

6.3.1 Summer case

In terms of forecast scores (not shown, but like Figures from 11 to 14) results are generally in favour of the 'standard' all-sky experiment, even though the other two experiments do not show any significant degradation. To investigate differences between the three experiments and justify the better performance of the 'standard' all-sky experiment, we rely on fits to other assimilated observations. This approach should be reliable and give us an estimation of the effectiveness of the new observations assimilated into the system. In fact, reduction in standard deviations of FG forecast departures is a sign that the system, assimilating new observations, is moving towards the right direction and, as a consequence, the resultant atmospheric background, which represents the short forecast range from the previous analysis, is improving. Water vapour sensitive channels from MHS (183 GHz channels), HIRS (channel 11 and 12) and IASI (channels above 1671) are actively assimilated into the system and, as a consequences, these instruments are good candidates to evaluate the impact of the assimilation of SSMI/S humidity sounding observations. Fits to MHS (from NOAA-18, NOAA-19 and Metop-A) and HIRS (from NOAA-19 and Metop-A) observations are analysed through Figure 18 and Figure 19. The overall result is that the 'standard' all-sky assimilation is globally beneficial because it provides better fits to the water vapour sensitive channels of other satellites.

It is interesting to point out the impact of SSMI/S channel 9 on the assimilation. Considering, respectively, the all-sky(SI10 ch9 denied) and the all-sky(SI10) experiment, we can estimate the influence of 183±7 GHz channel on the system. As expected, when SSMI/S channel 9 is removed, fits to the equivalent MHS channel 5 are worse than those provided by the all-sky(SI10) experiment, but also fits to MHS channel 3 and channel 4 are decreased. Degradations are also observed for HIRS channels 11 and 12. These results suggest the importance of assimilating 183±7 GHz, which is a lower tropospheric channel, but, most likely, overlaps the weighting functions of the upper troposphere channels of 183±3 and 183±1 GHz Considering fits to MHS observations, we can also infer that standard deviations are always

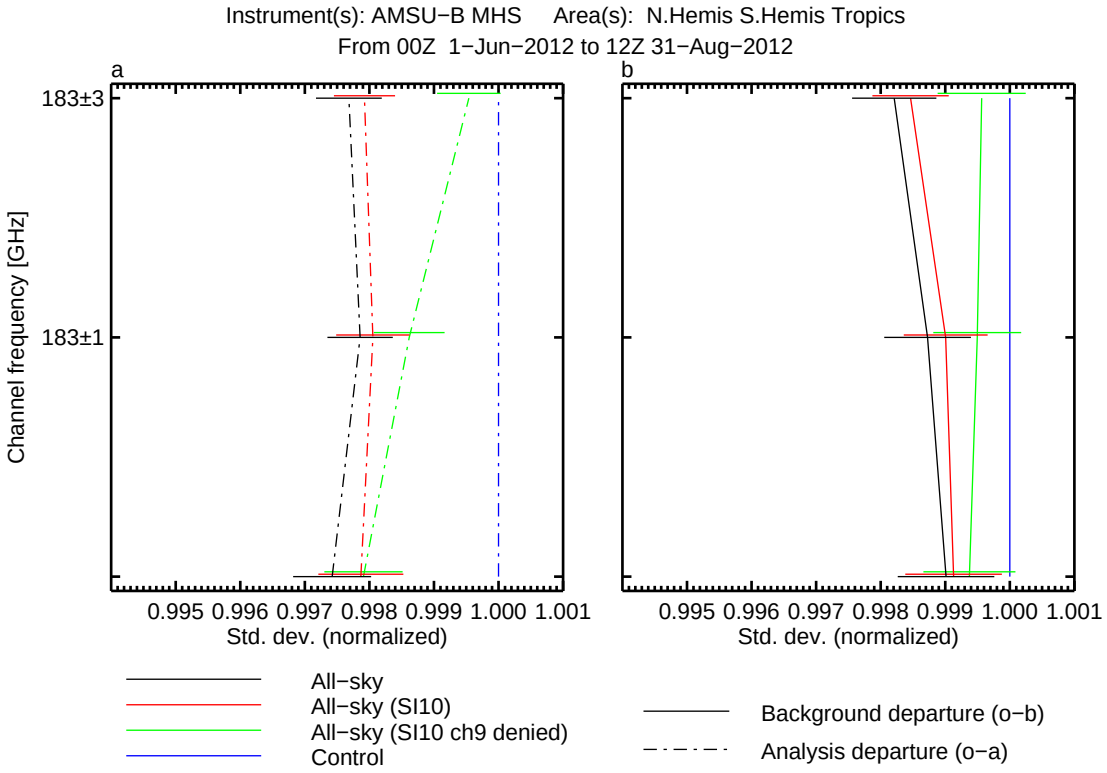

Figure 18: Normalised change in standard deviation of analysis departures (left) and FG forecast departures (right) for global MHS observations (from NOAA-18, NOAA-19 and Metop-A). Standard deviations are normalised by those of the control experiment. Error bars indicate the 95% confidence level. Statistics are for 3 months of period (June to August 2012).

smaller than the control experiment even though SSMI/S channel 9 is denied. This is an indication of the positive global impact of the two upper tropospheric humidity sounding channels on the assimilation system.

6.3.2 Winter case

Different conclusions can be drawn from the winter experimentation. In terms of forecast scores, the significant positive changes observed for the summer period are replaced by a general neutral impact. For instance, Figure 20 shows normalised change in RMS forecast error for vector wind at 200 hPa, 500 hPa and 850 hPa for the Southern (-90° to -20°) and Northern (20° to 90°) hemisphere. It would be difficult to conclude which experimentation produces better global scores: scores at longer ranges (from day 5 to day 8) can be considered in favour of the 'standard' all-sky experiment only in the Southern hemisphere, otherwise the outcome of the experiments can be roughly considered equivalent. These results might be explained considering different reasons. For instance, a larger number of observations is denied in the Northern hemisphere during winter time due to snow and high orography. We can also take into account that, as mentioned in section 4, the observation error formulation is slightly large and, as a consequence, observations might not have a big weight during the minimisation. The important overall result is that there is no evidence that the assimilation system is deteriorated in a particular way. Indeed, fits to conventional or other satellite humidity observations (plots not shown here) are always improved.

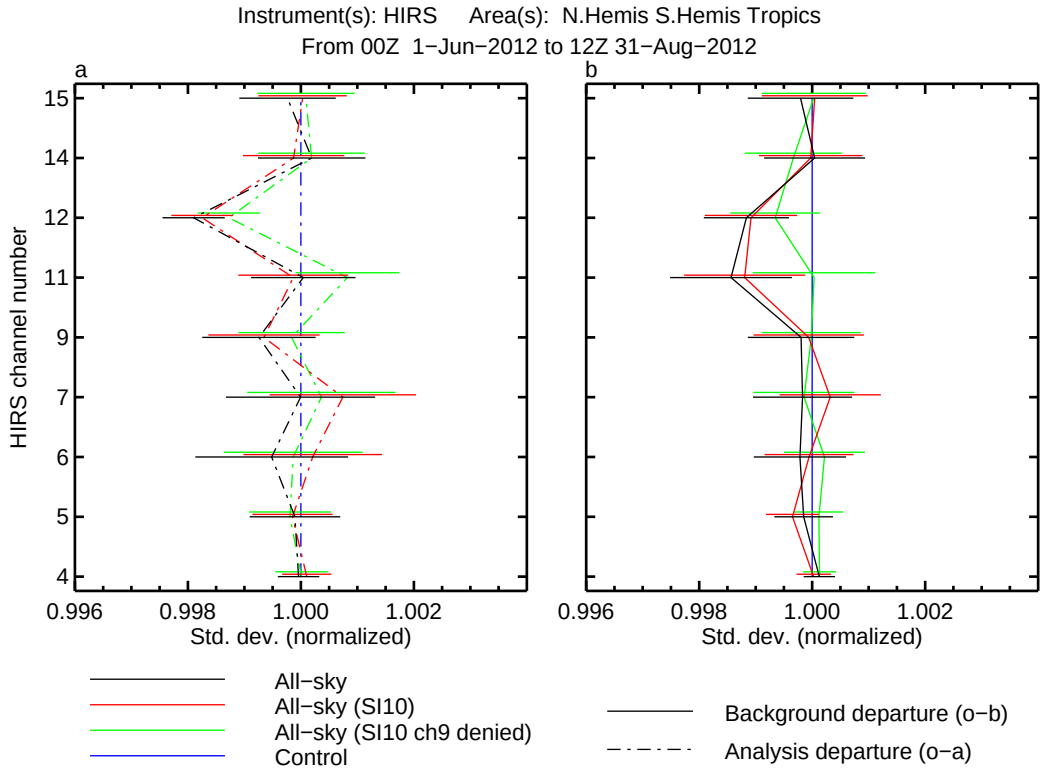

Figure 19: As Figure 18,but for global HIRS observations from NOAA-19 and Metop-A.

6.4 Surface screening impact

In this section, we briefly investigate the possibility of using a different surface screening criteria to discriminate which observations should be given to the 4D-Var minimisation. The surface to space transmittance (in the following also mentioned as tau screening) has been chosen to replace the surface temperature and orography screening (in the following also mentioned as MHS-like screening). The tau screening might allow a better observation coverage and be a more reliable guide as to which observations to discard according to the effective surface sensitivity. The 0.01 value has been estimated as a reasonable threshold to discard SSMI/S observations at 183 GHz channels: humidity sounding observations are rejected if the surface to space transmittance is greater than 0.01. Figure 21 compares the result of using the tau screening rather than the MHS-like, in terms of global number of SSMI/S observations which might be part of the variational analysis. Histograms of SSMI/S humidity sounding observations are obtained by binning the number of data as a function of latitude for summer and winter period (June and January 2012). Results are as expected: in channels 183±3 and 183±1 GHz (channels 10 and 11), where sensitivity to the surface is negligible, observation coverage is always improved, whilst at channel 9 (183±7 GHz), which is more affected by surface conditions, the number of observations decreases. The winter period (Figure 21 d,e,f) highlights differences between the two screening criteria: the number of observations at 183±7 GHz, in the Northern hemisphere, which is highly affected by surface variations during winter season, is reduced, while it is increased in the Southern hemisphere. The consistency between the two screening methods in channel 9 is also confirmed by the same number of observations which are taken into account between 40°N and 60°N. On the contrary, in this same region, in channels 10 and 11 MHS-like screening rejects the most of the data independently of the real channel surface sensitivity. The surface to space transmittance screening seems to be a good compromise for balancing

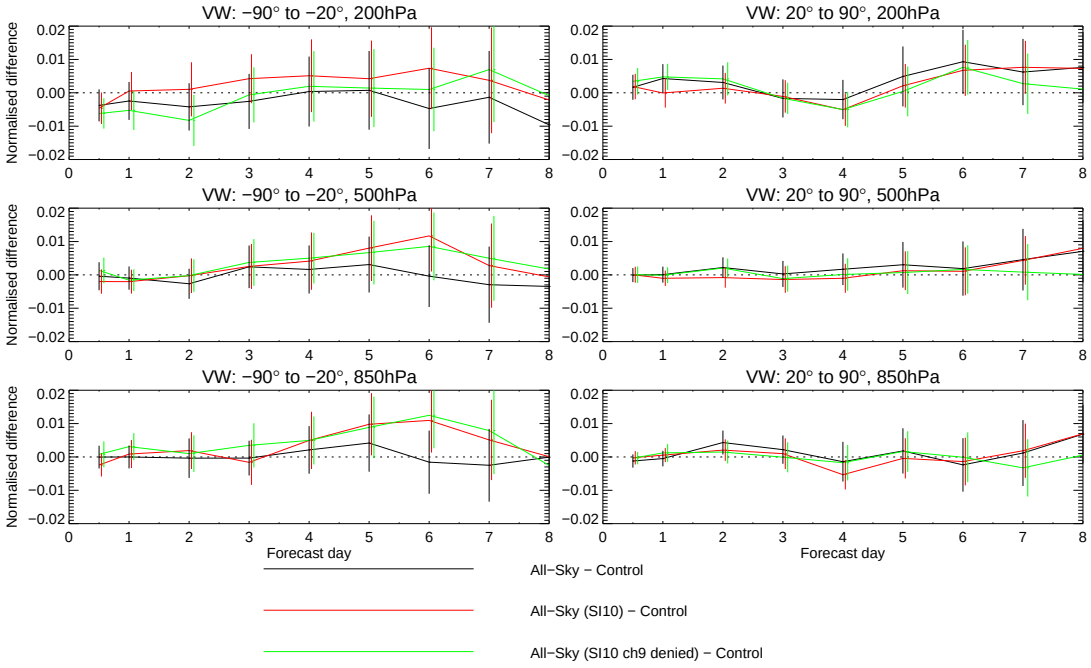

Figure 20: Normalised change in RMS forecast error in vector wind at 200 hPa (top row), 500 hPa (middle row) and 850 hPa (bottom row) for the Southern (-90° to -20°) and Northern (20° to 90°) hemisphere. Verification is against own analysis. Scores are based on a 3 months period, January to March 2012. Error bars indicate the 95% confidence level.

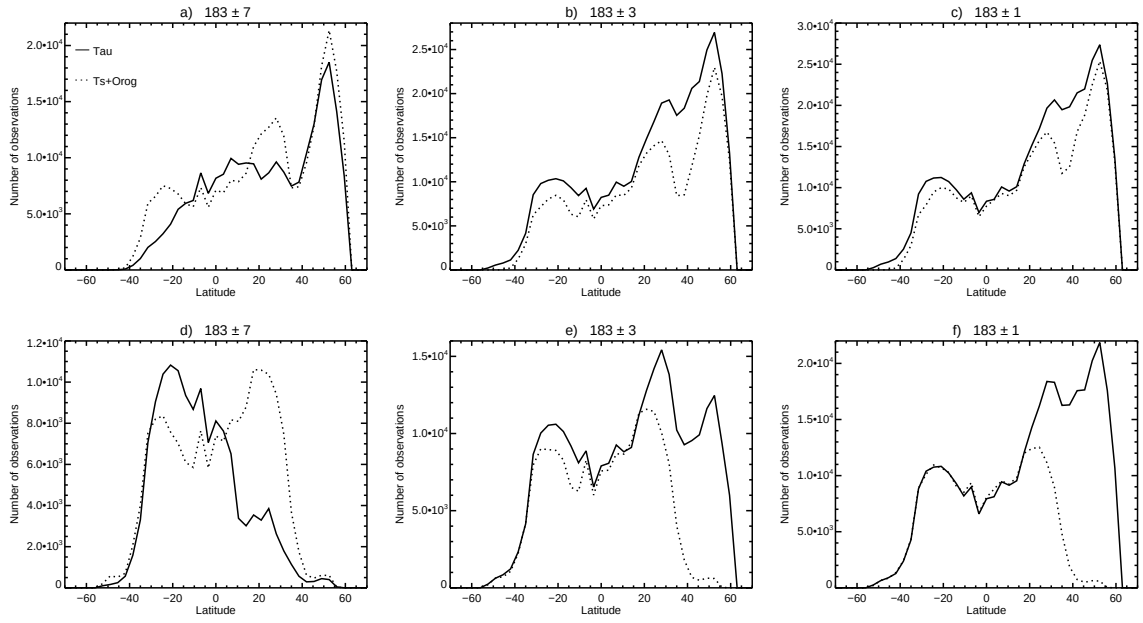

Figure 21: Number of SSMI/S humidity sounding observations in 3.5° latitude bins for the month of June (a,b,c) and January (d,e,f) 2012 using either transmittance screening (black line) or surface temperature and orography screening (dotted line).

the number observations at channel 9 and additionally extending the coverage at channels 10 and 11.

To analyse the impact of the different surface screening on the system, we ran an additional experiment, named all-sky(Tau), having same configuration of the all-sky experiment, but implementing the tau screening. Analysing the summer experimentation in terms of fits to other observations and forecast scores (plots not shown here), the tau screening approach shows reasonable results, even though the use of the MHS-like screening still produces the best statistics. We can again analyse through Figure 22 the change in RMS forecast error in winds comparing results between the all-sky and the all-sky(Tau). The assimilation system reacts positively to the tau screening, even though forecast scores plots show that the MHS-like screening brings a generally better result. The only difference in favour of the transmittance screening is the better scores, but not statistically significant, at longer ranges in the Southern hemisphere (from day 6 to day 8)

The assimilation system reacts completely different during the winter experimentation. Figure 23 examines change in RMS forecast error in winds for the winter experimentation. Both the Southern and Northern hemisphere are negatively affected by the extension of the observation coverage. In the Northern hemisphere, the main difference in terms of number of observations between the two experiment is at channel 183±3 and 183±1 GHz (Figure 21 e and f), hence, a larger number of observations available in the 4D-Var is not necessary a good thing. As mentioned before, the observation coverage of SSMI/S channels 10 and 11 is mainly extended between 40°N and 60°N. These areas of the Northern hemisphere during winter are most likely affected by possible snow or ice cover, rain or snow precipitation, low surface temperatures and high orography. Hence, residual surface contamination at 183±3 GHz might be the cause of degradation in forecast scores. In the Southern hemisphere, instead, the significant degradation in forecast scores at longer ranges (from day 4 to day 8) is most likely connected to the assimilation of a larger number of observations at SSMI/S channel 9 (Figure 21d) and, hence, to surface contamination issues. Using the transmittance screening, we are probably assimilating observations affected by

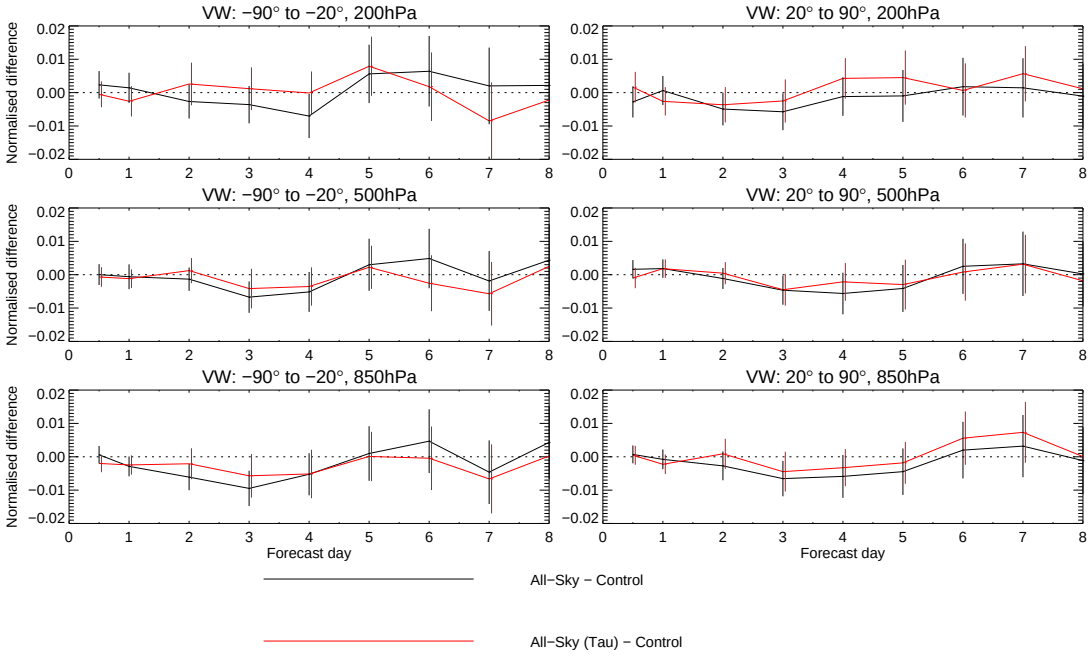

Figure 22: Normalised change in RMS forecast error in vector wind at 200 hPa (top row), 500 hPa (middle row) and 850 hPa (bottom row) for the Southern (-90° to -20°) and Northern (20° to 90°) hemisphere. Verification is against own analysis. Scores are based on a 3 months period, June to August 2012. Error bars indicate the 95% confidence level.

high orography and, as a result, the forecasts are biased. This behaviour is not observed in the Northern hemisphere for the equivalent season (summer experimentation Figure 22). The probable explanation is that observation coverage at 183±7 GHz in the Northern hemisphere (Figure 21a) is not extended as much as for the Southern hemisphere (Figure 21d), but actually is decreased.

In summary, the original MHS-like screening seems to be the most reliable way to assimilated SSMI/S humidity sounding observations over land. However, the use of transmittance screening might not be completely rejected. For instance, it might be considered to extend the observation coverage at 183±1 GHz, used with more cautious at 183±3 GHz and avoided at 183±7 GHz. It might also be interesting to investigate the possibility of considering the surface to space transmittance to model the observation error.

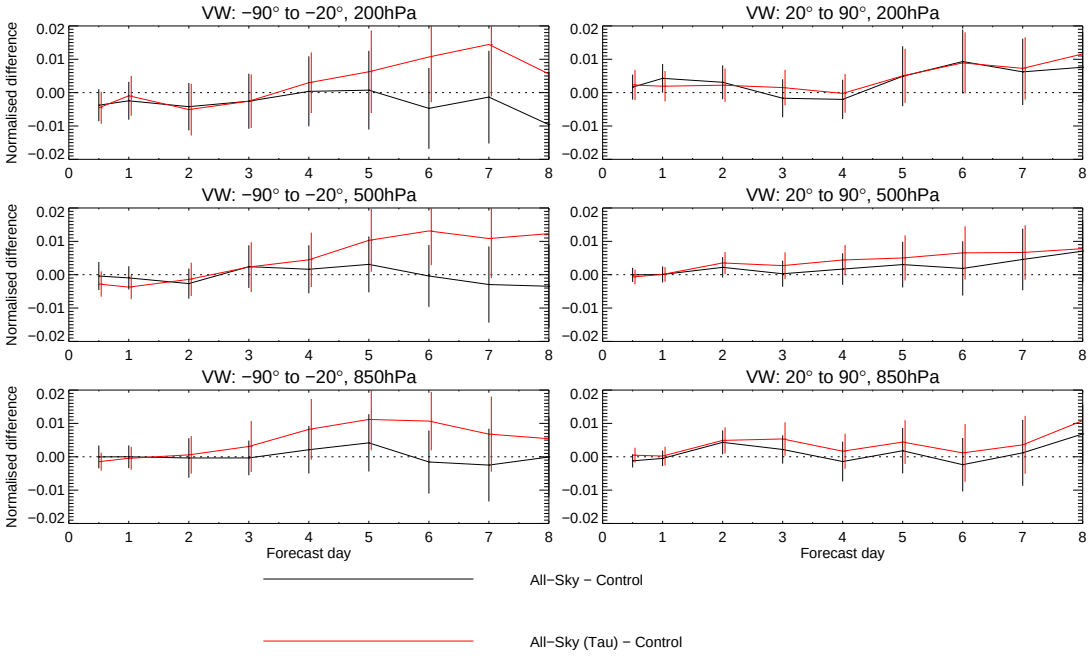

Figure 23: Same as Figure 22, but scores are for 3 months of winter period, January to March 2012.

7 Executive summary

This report investigates the possibility of achieving the assimilation of SSMI/S humidity sounding observations over land in all-sky conditions. Such a goal has required two distinct stages of development: one phase mainly oriented towards implementing the technical changes necessary to create the all-sky framework over land, and the second focused on the scientific evaluation of the impact on the assimilation system.

The technical and scientific developments can be considered as all the necessary changes which have to be done within the system before that any assimilation experiment can be run. The all-sky package over land is basically characterised by three main developments. Their important features can be summarised as follows:

Discrete dipole approximation (DDA) to represent optical properties of snow hydrometeors

Replacing inaccurate Mie sphere approach with more realistic DDA sector snowflakes largely improves the global simulation of microwave radiances. However, there is a difference to take into account between ocean and land surfaces. Over ocean, all-sky brightness temperatures are computed and weighted according the effective cloud fraction (‘Cav’ approach). Over land, instead, the best agreement between simulated and observed radiances is obtained when the effective cloud fraction is replace by the largest cloud fraction in the model profile (‘Cmax’ approach). This result is questionable considering the physical realism of the ‘Cav’ approach. However, one explanation might be in the forecast model bias between ocean and land: the model seems to produce less deep convection over land than over ocean in contrast to observations which indicate more convective areas over land. This might be the reason for the beneficial impact of the ‘Cmax’ approach over land which, as a result, helps to increase the amount of scattering producing colder simulated

brightness temperatures. The technical implementation within the IFS is also straightforward as long as the cloud overlap is varied from 'Cav' to 'Cmax' according to whether the surface is ocean or land. In conclusion, all the experimentation carried out over land in this paper implements the use of DDA sector snowflakes and 'Cmax' approach.

Observation error modelling

The all-sky assimilation over ocean predicts the total error of FG departures as a function of the symmetric cloud amount given by the average of observed and simulated polarisation difference at 37 GHz. To estimate the total error of FG departure over land we followed an equivalent approach, but the scattering index (SI) given by frequencies difference at SSMI/S channel 18 and channel 8 (respectively, 91 GHZ and 150 GHZ, horizontal polarisations) has been chosen as the symmetric predictor. This approach identifies two main areas: a region where the error can be estimated as a constant value and a second region, instead, where the error can be approximated by a linear fit. The first region can be interpreted as the clear-sky area where observations are unaffected by scattering and presumably free of cloud and precipitation. In this area, the total error for SSMI/S humidity sounding channels is constant and equal to 3 K. This error is comparable to the observation error used for the equivalent MHS channels which are assimilated in clear-sky conditions and have a 2 K error. The second region represents the all-sky conditions area where the influence of scattering, cloud and precipitation on observations increases, as well as the standard deviations of FG departures. The all-sky experimentation over land assimilate SSMI/S humidity sounding observations within these scattering areas.

Surface emissivity estimates

In the all-sky framework, emissivities are retrieved from satellite observations at window channels and then these estimations are assigned to higher frequencies according to the right polarisation in order to perform radiative transfer calculations. For instance, emissivities retrieved in SSMI/S channel 18 (91 GHz horizontal polarisation) are assigned to the humidity sounding channels. In order to take into account cloud contamination issues which might cause unrealistic emissivity estimates, emissivities from TELSEM are used to guide the choice of keeping or rejecting the retrieval. The biases observed globally suggest that FG emissivities have in average values 0.02-0.04 smaller than TELSEM estimations. The negative biases might be explained considering: a) the surface variability at the location and time of the observation (TELSEM is based on pre-calculated monthly mean emissivity climatology derived from ten-year SSM/I for clear-sky observations); b) the influence of cloud and precipitation in the retrieval scheme; c) resolution and frequency differences between SSMI/S and SSM/I.

Scientific impact of the all-sky assimilation over land has been evaluated by means of different assimilation experiments. To identify possible beneficial impact of the all-sky framework over land, all the relevant changes in the all-sky over ocean package have been taken into account within the control experiment. In this way, outcomes from any assimilation experiment over land can be reasonably evaluated as the result produced on top of the entire all-sky package over ocean. Control and assimilation experiments of SSMI/S 183 GHz channels over land were run at T511 horizontal resolution and 137 vertical levels in a 4D-Var 12 hour assimilation window. Results of the experimentation can be summarised as follows:

- First experimentation, covering 3 months of period from June to August 2012, (summer experimentation) has been done in order to compare results of the all-sky assimilation of SSMI/S humidity sounding channels to those provided by an equivalent 'cloud screening' experiment. The latter, implements the cloud contamination check (observations are rejected if the absolute difference between

observations and simulated clear-sky radiances in the 150 GHz channel is less than 5 K) and uses constant observation error of 2 K. Analysing forecast scores (normalised change in RMS forecast error for vector wind, relative humidity and geopotential height at 200 hPa, 500 hPa and 850 hPa for the Southern and Northern hemisphere), results generally favour the all-sky approach which brings positive changes through the atmosphere. All-sky is more effective at improving wind rather than relative humidity scores, confirming similar findings showed up when the SSMI/S 183 GHz channels were initially assimilated in the all-sky approach over ocean. The 4D-Var tracer effect is the probable cause of such improvements. While the system is already fed with many other microwave humidity sounding observations both over ocean and land, cloud and precipitation structures might lead to a better adjustments of the wind fields and, as a result, a small number of assimilated cloud affected observations might play an important rule in the wind analysis and forecast. The all-sky assimilation might bring into the system new observations assimilated over land, improving the analysis of the winds through the troposphere in the Southern hemisphere storm tracks, and, as a consequence, these improvements might be propagated into the polar regions during the forecast. Fits to conventional wind observations (TEMP-U and TEMP-V) and AMVs also confirm the positive impact of the all-sky approach.

- Reliability of the all-sky assimilation over land was additionally investigated by means of two other assimilation experiments which are characterised by same configuration of the all-sky experiment, but with a smaller number of assimilated observations. The goal is to evaluate the impact of assimilating: a) those observations affected by larger scattering index values (rejecting observations wherever SI is greater than 10 K); b) those observations which might be affected by surface conditions (blacklisting SSMI/S channel 9, 183$\pm$7 GHz). To make the statistics more significant, summer experimentation was also extended to 3 additional months of period from January to March 2012 (winter experimentation). Summer experimentation is always in favour of the all-sky assimilation whichever configuration is used in terms of both forecast scores and fits to other assimilated satellite humidity observations (MHS, HIRS, IASI). The analysis of fits to other humidity satellite observations suggest that assimilating the full set of SSMI/S humidity sounding channels in all-sky conditions is the most beneficial to the system. When channel 183$\pm$7 GHz is denied, fits to MHS 183$\pm$3 and 183$\pm$1 GHz and HIRS channels 11 and 12 are worse. Winter experimentation shows a general neutral impact in terms of forecast scores and analysing fits to conventional or other satellite observations there is no evidence that the assimilation system is deteriorated. Indeed, fits to other satellite humidity observations (MHS, HIRS, IASI) are always improved. It would be very difficult to identify those observations which might produce better or worse impact on the analysis and forecast scores. The causes of a neutral impact on forecast scores are not certain, but might for instance be due to the larger number of observations denied for the surface screening in the Northern hemisphere which is most likely affected by snow or ice cover, rain or snow precipitation, or low surface temperatures.

- The SSMI/S all-sky assimilation implements the surface screening based on surface temperature and orography thresholds as operationally adopted for the equivalent MHS humidity sounding channels. The possibility of using the surface to space transmittance to discriminate which observations should be included in the 4D-Var minimisation has been also investigated. The transmittance screening might be more reliable on which observations to discard according to the effective surface sensitivity. Histograms of the number of observations show that such screening seems to be a good compromise for reducing the number of data at channel 9, but extending the coverage at channels 10 and 11. RMS forecast errors in winds, for the summer experimentation, show that the assimilation system reacts positively to the transmittance screening. However, no significant changes are produced and forecast scores are generally in favour of the MHS-like surface temperature and orography screening. Results of the winter experimentation, instead, are definitely against the use of the transmittance screening. Residual surface contamination at 183$\pm$3 GHz and the larger number of surface sensitive observations

at 183±7 GHz are the probable causes of degradation in forecast scores, respectively, in the Northern and Southern hemisphere. For instance, forecasts might be biased by the assimilation of observations affected by high orography. In summary, the MHS-like screening seems to be the most reliable way to assimilated SSMI/S humidity sounding observations over land.

8 Conclusions

The overall outcome of this study not only demonstrates the feasibility of all-sky package over land, but also shows the beneficial impact on the system of assimilating humidity sounding channels in all-sky conditions. The significant positive impact on both forecasts scores and fits to other satellite observations in the summer experimentation, cannot be replicated in other all-sky experiments which implement a more cautious configuration. Experiments during the winter period, on one side, have a neutral impact in terms of forecast scores, but on the other side, confirm that the system is not deteriorated, but new useful data are supplied producing better fits to other satellite observations. More investigations might be done in order to work out the possibility of obtaining more impact on the assimilation system during winter period. The general indication is that it might worth analysing: a) surface screening and, hence, residual contamination issues; b) problems in the forecast model as well as the possibility of real physical differences between ocean and land surfaces in convection modelling. In any case, both the points are not linked to a particular deficiency of the all-sky package over land, but they are general conclusions which might help to better understand the assimilation of microwave radiances over land.

A new investigation has already started within the ECMWF system in order to validate the all-sky package over land discussed in this paper. Firstly, the all-sky assimilation of SSMI/S humidity sounding channels will be evaluated within the ECMWF 39r1 cycle. Summer experimentation covering 3 months of period, from June to August 2013, has been running and, even though the assimilation system has changed, it will provide a good reference to compare the reproducibility of the positive changes observed during the experimentation of summer 2012. Secondly, the all-sky package over land will be applied to MHS observations from NOAA-18, NOAA-19, Metop-A and Metop-B satellites. Experimentation to assimilate MHS observations in all-sky conditions over both ocean and land is in progress.

Acknowledgements

Fabrizio Baordo is funded through the EUMETSAT fellowship programme.

Acronyms

ATMS - Advanced Technology Microwave Sounder
DDA - Discrete Dipole Approximation
DMSP - Defence Meteorological Satellite Programme
IFS - Integrated Forecast System
MHS - Microwave Humidity Sounder
NOAA - National Oceanic and Atmospheric Administration
RTTOV - Radiative Transfer model for Television Infrared Observation Satellite Operational Vertical sounder
SSM/I - Special Sensor Microwave Imager
SSMI/S - Special Sensor Microwave Imager Sounder
TELSEM - Tool to Estimate Land Surface Emissivity at Microwave frequencies
TMI - TRMM Microwave Imager
TRMM - Tropical Rainfall Measuring Mission

References

Aires F., Prigent C., Bernado F., Jimnez C., Saunders R. and Brunel P., 2010. A tool to estimate Land Surface-Emissivities at Microwaves frequencies (TELSEM) for use in numerical weather prediction. Q. J. R. Meteorol. Soc. 137, 690–699.

Baordo F., Geer A. J. and English S., 2012. SSMI/S radiances over land in the all-sky framework: one year report. EUMETSAT/ECMWF Fellowship Programme Research Report No. 27, available from http://www.ecmwf.int.

Bauer P., Moreau E., Chevallier F. and OKeeffe U., 2006. Multiple-scattering microwave radiative transfer for data assimilation applications. Q. J. R. Meteorol. Soc. 132, 1259–1281.

Bauer P., Geer A. J., Lopez P. and Salmond D., 2010. Direct 4D-Var assimilation of all-sky radiances. Part I: Implementation. Q. J. R. Meteorol. Soc. 136, 1868–1885.

Bell, W., English, S.J., Candy, B., Atkinson, N., Hilton, F., Baker, N., Swadley S.D., Campbell, W.F., Bormann, N., Kelly, G. and Kazumori, M., 2008. The assimilation of SSMIS radiances in numerical weather prediction models. IEEE Transactions on Geoscience and Remote Sensing, v.46, p.884–900.

Bennartz, Thoss, Dybbroe and Michelson, 2002. Precipitation analysis using the Advanced Microwave Souunding Unit in support of nowcasting applications. Meteorol. Appl., 9, 177–189.

Bennartz R. and Bauer, P., 2003. Sensitivity of microwave radiances at 85–183 GHz to precipitating ice particles. Radio Sci. 38, 8075.

Geer A. J., Bauer P. and ODell C.W., 2009. A revised cloud overlap scheme for fast microwave radiative

transfer in rain and cloud. J. Applied Meteorology, 48, 2257–2270.

Geer A. J. and Bauer P., 2010. Enhanced use of all-sky microwave observations sensitive to water vapour, cloud and precipitation. Published simultaneously as ECMWF Technical Memoranda 620 and ECMWF/EUMETSAT fellowship reports 20.

Geer A. J., Bauer P. and Lopez P., 2010. Direct 4D-Var assimilation of all-sky radiances: Part II. Assessment. Q. J. R. Meteorol. Soc. 136, 1886–1905.

Geer A. J. and Bauer P., 2011. Observation errors in all-sky data assimilation. Q.J.R. Meteorol. Soc. 137: 2024–2037.

Geer A. J., Bauer P. and English S., 2012. Assimilating AMSU-A temperature sounding channels in the presence of cloud and precipitation. ECMWF, available from http://www.ecmwf.int.

Geer A. J. and Baordo F., 2013. Improved scattering radiative transfer for frozen hydrometeors at microwave frequencies. To be submitted.

Geer A. J., 2013. All-sky assimilation: better snow-scattering radiative transfer and addition of SSMI/S humidity sounding channels. To be submitted.

Joseph J., Wiscombe W. J. and Weinman J. A., 1976. The delta-Eddington approximation for radiative flux transfer. J. Atmos. Sci. 33, 2452–2459.

Kummerow C., Barnes W., Kozu T., Shiue J. and Simpson J., 1998. The Tropical Rainfall Measuring Mission (TRMM) sensor package. J. Atmos. Ocean. Tech. 15, 809–817.

Kunkee D.B., Poe G.A., Boucher D.J., Swadley S.D., Hong Ye., Wessel J.E. and Uliana E.A., 2008. Design and evaluation of the first Special Sensor Microwave Imager/Sounder. IEEE Trans. on Geoscience and Remote Sensing, 43, 5, 948–959.

Liu G., 2008. A database of microwave single-scattering properties for non spherical ice particles. Bull. Am. Met. Soc. 111, 1563–1570.

Liu Q., Weng F. and English S., 2011. An Improved Fast Microwave Water Emissivity Model. IEEE Trans. on Geoscience and Remote Sensing, 49, 4, 1238–1250.

O'Dell C.W., Bauer P. and Bennartz R., 2007. A fast cloud parametrization for microwave radiance assimilation. J. Atmos. Sci. 64, 3896–3909.

Prigent C., Chevallier F., Karbou F., Bauer P. and Kelly G., 2005. AMSU-A surface emissivities for numerical weather prediction assimilation schemes. J. Applied Meteorology, 44, 416–426.

Sun N. and Weng F., 2008. Evaluation of Special Sensor Microwave Imager/Sounder (SSMI/S) Environmental Data Records. IEEE Transactions on Geoscience and Remote Sensing. 46, no. 4.